

INVESTIGATION OF DEEP LEVEL IMPURITIES
(OXYGEN AND CHROMIUM) IN BULK GALLIUM ARSENIDE
AND Au-GaAs SCHOTTKY DIODES

By

CHERN I HUANG

A DISSERTATION PRESENTED TO THE GRADUATE
COUNCIL OF THE UNIVERSITY OF FLORIDA IN PARTIAL
FULFILLMENT OF THE REQUIREMENTS FOR THE DEGREE OF
DOCTOR OF PHILOSOPHY

UNIVERSITY OF FLORIDA
1973

ACKNOWLEDGMENTS

The author wishes to express his sincere appreciation to the members of his supervisory committee: Dr. S. S. Li, Dr. F. A. Lindholm, Dr. E. R. Chenette, Dr. A. D. Sutherland and Dr. T. A. Scott for their guidance and encouragement throughout this research. The author also gratefully acknowledges the helpful discussions with Dr. C. T. Sah.

The research that resulted in this dissertation was part of a larger effort; therefore, the author is indebted to his fellow co-workers for their generous cooperation, and, in particular, the author wishes to mention H. F. Tseng, R. F. Motta, T. H. Smith, W. A. Lukaszek and C. F. Hiatt.

The author acknowledges the competence of Mrs. Vita Zamorano who typed this manuscript.

This investigation was supported by the Advanced Research Projects Agency, U. S. Department of Defense and monitored by the Air Force Cambridge Research Laboratories under contract No. F19628-72-C-0368.

TABLE OF CONTENTS

	Page
ACKNOWLEDGMENTS	ii
LIST OF TABLES	v
LIST OF FIGURES	vi
LIST OF SYMBOLS	viii
ABSTRACT	xi
Chapter	
I. INTRODUCTION	1
II. CURRENT TRANSPORT IN SCHOTTKY BARRIER DIODES	5
Introduction	5
Current Transport Theory	5
Interfacial Layer Effect	8
Field Dependence of the Barrier	9
Surface States Effect	11
III. THE CAPACITANCE-VOLTAGE CHARACTERISTICS OF SCHOTTKY BARRIER DIODES IN THE PRESENCE OF DEEP LEVEL IMPURITIES	13
Introduction	13
Review of the Existing Models	14
Transition Processes in Deep Impurity Centers	17
Dark Transient Capacitance	19
Transient Photocapacitance	22
Summary	23
IV. RECOMBINATION AND TRAPPING PROCESSES IN BULK n-TYPE GaAs IN THE PRESENCE OF DEEP LEVEL IMPURITIES	24
Introduction	24
Charge Neutrality in Semiconductors	25
Trapping and Recombination Processes Through Deep Level Impurities	27
Radiative Recombination in the Host Crystal	30

TABLE OF CONTENTS (Continued)

Chapter	Page
IV. Continued	
Carrier Lifetime Measurement Using PME and PC Effects	31
Summary	34
V. EXPERIMENTS	35
Preparation of Devices	35
Sample Preparation	35
Current-Voltage Measurement	37
Capacitance-Voltage Measurement	37
Photocapacitance Measurement	40
Bulk Effect Measurements	40
VI. EXPERIMENTAL RESULTS AND ANALYSES	43
Introduction	43
Forward Current-Voltage Measurement of Au-GaAs	
Schottky Diodes	43
Reverse Current-Voltage Measurement of Au-GaAs	
Schottky Diodes	48
Transient Capacitance Measurement of Au-GaAs	50
Hall-Effect and Conductivity Measurement	58
PME and PC Measurement on Chromium-doped n-type GaAs	59
PME and PC Measurement on Oxygen-doped n-type GaAs .	64
VII. CONCLUSIONS	68
Summary	68
Suggestions for Further Study	70
BIBLIOGRAPHY	71
BIOGRAPHICAL SKETCH	73

LIST OF TABLES

Table		Page
1.	Basic physical parameters of typical Au-GaAs (n-type) Schottky barrier diodes at 300°K	36
2.	Summary of the results for Au-GaAs (n-type) Schottky barrier diodes deduced from transient dark and photo-capacitance measurements	56

LIST OF FIGURES

Figure	Page
1. Energy band diagram of a metal-semiconductor (n-type) contact with an interfacial layer and surface states (After Cowley and Sze, Reference 21)	6
2. (a) Energy band diagram of a metal-semiconductor (n-type) contact with the presence of donor-type deep level impurities	
(b) Spatial distribution of charges	16
3. The energy band diagram and (a) four thermal and (b) four optical transition processes between the deep level impurity and the conduction band (After Sah et al., Reference 15)	18
4. Localized states introduced by the shallow and deep level impurities in the forbidden band for a semiconductor. The centers are shown in their available charge states	26
5. Energy band diagram for a semiconductor doped with deep level acceptor impurities in thermal equilibrium and under steady-state illumination: (a) thermal equilibrium; (b) intermediate injection; (c) high injection	28
6. Test set-up for measuring Schottky barrier diode current-voltage characteristics	38
7. Experimental set-up for measuring transient dark and photocapacitance of the metal-GaAs Schottky barrier diodes	39
8. Experimental set-up for the AC PME measurement	41
9. Forward current-voltage relationship of Au-GaAs (n-type) Schottky diode D-11 at various temperatures	45
10. Forward current-voltage relationship of Au-GaAs (n-type) Schottky diode D-17 at various temperatures	46

LIST OF FIGURES (continued)

Figure		Page
11.	I_s/T^2 versus $10^3/T$ for the Au-GaAs (n-type) Schottky barrier diodes D-11 and D-17	47
12.	Reverse voltage-current relationship for the Au-GaAs Schottky barrier diode D-17	49
13.	The actual measured capacitance as a function of time	51
14.	The thermal emission rate of electrons as a function of average electric field. The subscript pH denotes that the transient photocapacitance method was being employed to obtain the data	52
15.	The thermal emission rate of electron as a function of temperature ($10^3/T$) between 285 and 316°K. The data were taken at $V = -6$ volts	54
16.	A plot of C^{-2} as a function of reverse bias voltage for D-17, D-7 and D-11. The superscript ° represents the values taken at $t = 0^+$	57
17.	The photo-Hall mobility versus photoconductance for sample S-3 at 20.8 and 4.2°K	60
18.	The PME short-circuit current per unit width of sample per unit magnetic flux density, I_{PME}/B , versus photoconductance ΔG for samples S-1 and S-2 at 80 and 300°K	61
19.	The PME apparent lifetime τ_a , the electron lifetime τ_n and the hole lifetime τ_p versus photoconductance ΔG at 80 and 300°K	63
20.	The PME short-circuit current per unit width of sample per unit magnetic field intensity, I_{PME}/B , versus photoconductance for oxygen-doped sample S-3 at 20.8 and 4.2°K	65
21.	The PME apparent lifetime τ ($\tau_a = \tau_n = \tau_p$) versus photoconductance ΔG for S-3 ^a at 20.8°K and 4.2°K ...	67

LIST OF SYMBOLS

A	Area of the Schottky diode
A^*	$\frac{4\pi q m^* k^2}{h^3}$
B	Magnetic flux density
B_r	Capture probability of electron for direct band gap semiconductor (see Eq. (45))
b	μ_n/μ_p
C, C_i	Capacitance of a capacitor in general and at bias voltage V_i respectively
c_n^o, c_p^-	Capture rate of neutral and negative impurities respectively
c_n, c_p	Total electron and hole capture rates respectively
D_a, D_n, D_p	Effective, electron and hole diffusion constants respectively
D_s	Surface state density
d	Thickness of the bulk sample
E_C, E_V	Conduction and valence band edges respectively
E_f, E_g	Quasi-Fermi level and energy band gap of a semiconductor respectively
E_T	Thermal activation energy of deep level impurity
E	Electric field intensity
e_n, e_p	Electron and hole thermal emission rates respectively
ϵ, ϵ_i	Dielectric constants of the semiconductor and the interfacial layer respectively
ΔG	Photoconductance
h	Plank's constant

I_{PME}	PME short-circuit current
I, I_{sat}	Current and saturation current respectively
J, J_{sat}	Current and saturation current densities respectively
k	Boltzmann's constant
κ, ℓ	See Eqs. (40) and (42)
m	Diode voltage dividing factor (see Eqs. (3) and (10))
m_o, m^*	The free and effective masses of electron respectively
m_e, m_h	The density of states effective masses for electron and hole respectively
N_C, N_V	Effective density of states for the conduction and valence bands respectively
N_D	Density of shallow donor
N_T	Density of deep level impurity
N_T^-, N_T^o	Density of negative and neutral deep impurities respectively
n_D	Density of unionized shallow donor
n, p	Nonequilibrium electron and hole densities respectively
n_o, p_o	Thermal equilibrium electron and hole densities respectively
n_i	Intrinsic carrier concentration
n_1, p_1	Effective electron and hole densities respectively when the Fermi-level coincides with the trap level
$\Delta n, \Delta p, \Delta n_D, \Delta N_T, \text{etc.}$	Excess densities over respective thermal equilibrium densities
Δn_o	Excess carrier density at the illuminated surface
n_T, p_T	Electron and hole concentrations at the deep impurity centers respectively
q	Electronic charge
ΔQ	Variation of charge density
R	Recombination rate (see Eqs. (41) and (46))

r	Resistance
γ	$\frac{C_n^o}{C_p^-}$
S_n, S_p	Electron and hole capture cross section respectively
T	Temperature
Γ	See Eq. (40)
$\tau_\infty, \tau_n, \tau_p, \tau_a$	Large injection carrier, electron, hole and apparent PME lifetimes respectively
μ_n, μ_p, μ_H	Electron, hole and Hall mobilities respectively
V, V_R	Applied voltage and reverse bias voltage respectively
V_{bi}, V'_{bi}	Diffusion potential (see Fig. 1) and apparent diffusion potential respectively
V_e	See Eq. (8)
v_t	Electron thermal velocity
$\phi_a, \phi_b, \phi_{bo}$	Apparent, actual and intrinsic barrier heights of metal-semiconductor Schottky diode respectively
ϕ_o	Energy level at the surface (see Fig. 1)
ϕ_t	See Eq. (22b)
λ_o	See Fig. 2(a)
λ_i	Thickness of the interfacial layer (see Fig. 1)
x_t	See Fig. 2(a)
χ	Electron affinity
α	$\frac{e_n}{e_n + e_p}$
$\rho(x)$	Charge density
W	Depletion layer width
Δ	Potential across interfacial layer (see Fig. 1)

Abstract of Dissertation Presented to the
Graduate Council of the University of Florida in Partial
Fulfillment of the Requirements for the Degree of Doctor of Philosophy

INVESTIGATION OF DEEP LEVEL IMPURITIES
(OXYGEN AND CHROMIUM) IN BULK GALLIUM ARSENIDE
AND Au-GaAs SCHOTTKY DIODES

By

Chern I. Huang

March, 1973

Chairman: S. S. Li

Major Department: Electrical Engineering

The roles that the deep level impurities, chromium and oxygen, play in the recombination and trapping processes of the photoinjected carriers in bulk n-type GaAs have been investigated by using photo-magnetoelectric (PME) and photoconductive (PC) effects at various injection ranges and temperatures. A generalized theory for the PME and PC effects is developed, taking into account the variation of carrier lifetimes with injected carrier density and the trapping of holes in the chromium levels, by using a Shockley-Read type recombination and trapping model. The experimental results have yielded the dependence of the carrier lifetimes on injections over a wide injection range in the Cr-doped GaAs. For the oxygen-doped n-type GaAs, it is found that at low temperatures the band to band radiative recombination mechanism prevails. The experimentally obtained capture probability compares favorably with Hall's radiative recombination model.

The electronic properties of oxygen and chromium impurities in n-type GaAs such as the thermal activation energies, the thermal emission rate, the capture cross section of electrons and the dependence of the thermal emission rate on static electric fields are obtained from the transient dark and photocapacitance measurements on the Au-GaAs Schottky barrier diodes in which the GaAs substrates are doped either with oxygen or chromium.

CHAPTER I

INTRODUCTION

Since gallium arsenide (GaAs) has shown superior electrical properties, such as high electron mobility, high breakdown field and lower shallow level impurity ionization energy over those of silicon, better understanding of its physical properties has become an enthusiastically pursued subject.

In reality and potentiality, GaAs finds wide application in solid state devices. The device characteristics are greatly influenced by the existence of deep level impurities in GaAs which is either inherited from the crystal growing processes or intentionally doped. The situation is similar to that of gold-doped silicon. The progress in the applications of GaAs, where the concentration of a deep level impurity is abundant, will be furthered by a complete understanding of its electrical properties. In this material the impurity centers make a substantial contribution to the density of charge centers that fluctuate with carrier injection. This is due to its ability to communicate with the excess electrons in the conduction band of the semiconductor.

Although considerable work has been published concerning the trapping and recombination properties of defects in semiconductors, relatively few are dealing with GaAs. The most effective method for studying the trapping and the recombination mechanisms is the carrier

lifetime measurement. Among available methods, the photomagneto-electric (PME) and the photoconductive (PC) effect measurements performed under steady-state condition are the favorite ones for obtaining the excess carrier lifetimes and consequently for understanding the transport mechanism.

The PME and PC effects in undoped semi-insulating and semi-conducting GaAs single crystals were first reported by Holeman and Hilsum.¹ Hurd² reported the experimental results of the Dember and PME effects in oxygen-doped GaAs between 140 and 300°K. The photo-electronic analysis of high resistivity n-type GaAs was given by Bube.³ It has also been shown that the minority carrier lifetimes of the more heavily doped samples are controlled by band to band radiative recombination, while the minority carrier lifetimes of high resistivity samples are determined by recombination centers lying in the middle of the band gap.^{4,5} A more recent study on the photoconductivity of high resistivity GaAs and Cr-doped GaAs was given by Broom.⁶ In all these works, the roles that oxygen and chromium have played in the excess carrier recombination and trapping have not been specifically determined. There is lack of understanding about the basic physical properties of the deep impurity centers which is believed to have caused high resistivity in GaAs.⁷

Most recently, the properties of deep level impurity in GaAs have received noticeable attention in the literature. It has also become clear that the metal-semiconductor Schottky diode is a powerful tool in obtaining fundamental deep impurity parameters through its time-varying capacitance-voltage relationship.

With respect to the understanding of semiconductor properties via Schottky barrier diodes, Goodman⁸ presented the first comprehensive descriptions of the contact characteristics in terms of the capacitance-voltage relationship of the diode. Although the deep level impurity effect was included, no detailed transient consideration was given in his treatment. However, an interesting transient behavior in the high frequency capacitance of the Schottky barrier diode on n-type GaAs was observed.^{9,10,11,12} This behavior has been interpreted as a result of the existence of deep level impurities in GaAs. The electron capture cross section, the thermal emission rate of electrons and the thermal activation energy of deep impurity can presumably be obtained from the transient time constant.^{9,10,11,12} However, the results for GaAs are not in good agreement. For example, the determined thermal activation energy for oxygen in n-type GaAs ranges from 0.57 eV¹³ to 0.9 eV¹¹ from the conduction band edge, comparing with the value of 0.8 eV obtained by optical and Hall-effect measurements.¹⁴

Sah et al.¹⁵ reported transient capacitance experiments using gold-doped silicon p-n step junctions (either p^+n or n^+p junction). According to their model, the electronic properties of impurity centers in semiconductors such as energy level, multiplicity of charge state, thermal and optical capture cross sections, and emission rates of electrons can be obtained. Their model applies equally well to the metal-semiconductor Schottky barrier diodes. In this work, the Au-GaAs (n-type) Schottky barrier diodes are fabricated with substrates doped either with oxygen or chromium. The transient capacitance experimental results are analyzed by using the model proposed by Sah et al.

The objective of this research is to study the transport, recombination and trapping mechanisms of steady-state photoinjected carriers associated specifically with oxygen and chromium impurities. The electronic properties of these impurity centers, such as thermal activation energy, thermal emission rate, capture cross section of electrons and dependence of the thermal emission rate on static electric fields are also investigated.

In Chapter II, the current transport theory of the metal-semiconductor Schottky barrier diode is studied. Since the low carrier concentration ($n = 10^{14} - 10^{15} \text{ cm}^{-3}$) n-type GaAs substrates have been used for diode construction, it is expected that the depletion layer of the diodes will be relatively wide. Therefore, the most probable mechanism of electron transport at the interface is by thermionic emission over the barrier. Being limited by imperfect GaAs technology, the diodes fabricated are not ideal. Thus the interfacial layer and surface state effects are also considered. In Chapter III, following a brief review of the existing transient capacitance models, the method for determining the deep impurity physical properties is discussed. Chapter IV contains recombination models describing the excess carrier behavior in the presence of deep impurities. The experimental procedures are described in Chapter V. Chapter VI gives the experimental results and their analyses. Conclusions and suggestions for further study are given in Chapter VII.

CHAPTER II

CURRENT TRANSPORT IN SCHOTTKY BARRIER DIODES

Introduction

The current transport in metal-semiconductor barriers is mainly due to majority carriers in contrast to p-n junctions where the minority carriers are responsible. The theory of current flow over the barrier of metal-semiconductor contacts is complicated. There are several mechanisms, namely, thermionic emission,¹⁶ diffusion,^{16,17} thermionic emission-diffusion,¹⁸ thermionic-field emission and field emission.¹⁹ There are also some factors such as interfacial layer,^{20,21} surface states^{22,23} and image force lowering of the barrier²⁴ that could cause deviations from the ideal case. The energy band diagram of such a physical system is shown in Fig. 1. However, the identification of these factors with current-voltage characteristics of a Schottky barrier diode has been extremely difficult. Generally, one must specify the range of applied bias voltage and temperature before a relationship among current, voltage and temperature can be established.

Current Transport Theory

Ignoring the effect of image force and electron collisions within the depletion region, Bethe's thermionic emission theory¹⁶ gives

$$J = A^*T^2 \exp\left(\frac{-q\phi_b}{kT}\right) \left[\exp\left(\frac{qV}{kT}\right) - 1\right] \quad (1)$$

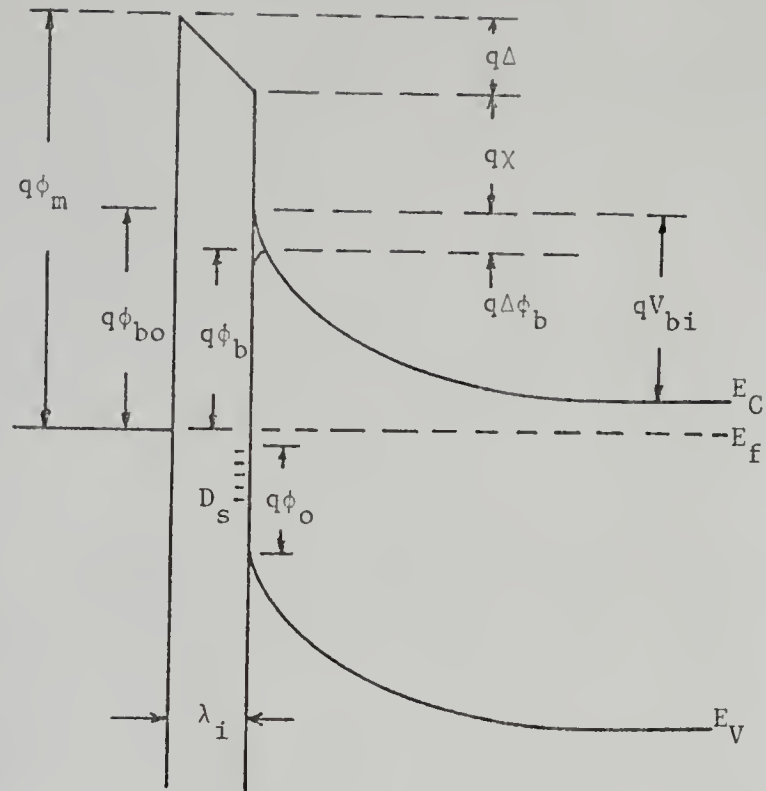


Fig. 1 Energy band diagram of a metal-semiconductor (n-type) contact with an interfacial layer and surface states. (After Cowley and Sze, Ref. 21)

where

$$A^* = \frac{4\pi q m^* k^2}{h^3}$$

Assuming that the carrier concentration at the metal-semiconductor interface and the edge of the depletion region are unaffected by the current flow, the total current derived from the diffusion theory¹⁷ is

$$J = \left(\frac{q^2 D_n N_C}{kT} \right) \left[\frac{q(V_{bi} - V) 2N_D}{\epsilon} \right]^{1/2} \left[\exp\left(\frac{-q\phi_b}{kT}\right) \right] \left[\exp\left(\frac{qV}{kT}\right) - 1 \right] \quad (2)$$

where the electron collisions are considered.

Crowell and Sze¹⁸ incorporated Schottky's diffusion theory and thermionic emission theory into a single thermionic-diffusion theory. A low electric field limit for application of this theory is estimated from consideration of phonon-induced back scattering near the potential energy maximum. A high electric field limit associated with the transition to thermionic field emission is obtained by considering the effect of quantum-mechanical reflection and quantum tunneling on the thermionic recombination velocity near the metal-semiconductor interface. It gives

$$J = J_{sat} \exp\left\{ \frac{2(m-1)}{m} \cdot \frac{qV_{bi}}{kT} \left[\left(1 - \frac{V}{V_{bi}}\right)^{1/2} - 1 \right] \right\} \left[\exp\left(\frac{qV}{kT}\right) - 1 \right] \quad (3)$$

where

$$m = \left(\frac{q}{kT} \right) \frac{dV}{d(\ln J)} \quad (4)$$

$$J_{sat} = A^* T^2 \exp\left(\frac{-q\phi_b}{kT}\right) \quad (5)$$

The value of m is determined by the type of emission over or through the potential barrier. For pure thermionic emission $m \rightarrow 1$. For other cases m takes on a more complicated form.

Another derivation has been given by Padovani and Stratton¹⁹ covering the cases of thermionic-field emission and field emission. The temperature dependence of current flow over a Schottky barrier is fully discussed.

Since the carrier concentration of GaAs used in this work is in the order of $10^{14} \sim 10^{15} \text{ cm}^{-3}$, the depletion layer width for Au-GaAs (n-type) Schottky barrier is of the order of $100 \mu\text{m}$ at zero bias. Accordingly, the most probable mechanism of electron transport is by thermionic emission. In the later part of this chapter, the thermionic emission theory will be explored further.

Experimental evidence indicates that the metal-GaAs surface has a peak density of surface states near one third of the band gap from the valence band edge.²² The presence of surface states causes field dependence of the barrier height.²³ This in turn affects the C-V^{18,25} and I-V characteristics of the diode. Because of the imperfect GaAs technology, there exists an interfacial layer between metal and GaAs. Experimental results have connected the barrier height of the Schottky diode with thickness of the interfacial layer.²⁰ Thus the surface states and interfacial layer effects will also be discussed.

Interfacial Layer Effect

The metal contacts evaporated onto the chemically etched surface under the ordinary laboratory conditions cannot be thought to be ideally intimate; there exists an interfacial layer.^{20,26} The thickness of the layer is estimated to be $5 \sim 30 \text{ \AA}$. It has been assumed by many authors, for simplicity, that the layer is electrically transparent.¹⁹ This is true under high electric field.^{18,27} The current-voltage relation at

very low bias voltage has been overlooked. Simmons²⁷ derived a formula for the electric tunneling effect through a potential barrier of arbitrary shape existing in a thin insulating film.

For very low applied voltage, the tunneling resistivity is constant (i.e., contact is ohmic). The interfacial layer can be treated as a high resistance series resistor. Its resistance value depends on the thickness of the layer, equivalent barrier height and dielectric constant of the layer.^{27,28}

In view of this ohmic behavior, the thermionic emission theory gives

$$J = A^*T^2 \exp\left(-\frac{q\phi_b}{kT}\right) \left[\exp\left(\frac{qV}{mkT}\right) - 1\right] \quad (6)$$

where m is a voltage dividing factor. It is worth noting that m is essentially a function of interfacial layer resistivity and Eq. (6) is valid for low reverse bias voltage. At very low voltage, $V \ll \frac{mkT}{q}$, Eq. (6) becomes

$$J = A^*T^2 \exp\left(-\frac{q\phi_b}{kT}\right) \left(\frac{qV}{mkT}\right) \quad (6a)$$

which shows a linear relation between J and V .

Field Dependence of the Barrier

As mentioned in the previous section, the interfacial layer plays an important role at very low bias voltage. At high reverse voltage, Eq. (6) becomes

$$J = A^*T^2 \exp\left(-\frac{q\phi_b}{kT}\right) \quad (7)$$

which predicts that the reverse current would exhibit saturation. However, this prediction is not consistent with the experimental

results.^{18,19,29} It is found that the potential barrier ϕ_b is slightly dependent upon the applied electric field.

Among barrier lowering mechanisms, the image force barrier lowering gives²⁴

$$(\Delta\phi_b)_{\text{image}} = \left(\frac{qE}{4\pi\epsilon}\right)^{1/2} \quad (8)$$

where

$$E = \left(\frac{2qN_D V_e}{\epsilon}\right)^{1/2}$$

$$V_e = \phi_b - V - \frac{kT}{q} \left(1 + \ln \frac{N_C}{N_D}\right)$$

On the other hand, the barrier lowering due to the equilibrium electrostatic charge distribution (dipole layer) prevailing at the contact can be expressed as²⁹

$$(\Delta\phi_b)_{\text{static}} \cong \alpha E + \dots \quad (9)$$

Here a Maclaurin series expansion is used and α is an adjustable empirical parameter.

Combining Eqs. (6), (8) and (9), the reverse current is given by

$$J = A^*T^2 \exp \left[\frac{q}{kT} \left(-\phi_{bo} + \left(\frac{qE}{4\pi\epsilon} \right)^{1/2} + \alpha E \right) \right] \left[\exp \left(\frac{qV}{mkT} \right) - 1 \right] \quad (10)$$

This equation should be able to cover the current-voltage behavior in a wide voltage range and for various physical situations. Andrews and Lepselter²⁹ used this model successfully to explain the I-V characteristics of metal-silicide Schottky diodes. Since their diode fabrication process virtually eliminates the interfacial layer, the value of m is nearly equal to unity.

Surface States Effect

The effect of surface states on the current transport is shown in the form of barrier height lowering. Crowell et al.²³ have obtained

$$\frac{d\phi_b}{dE} = - \left[\frac{qD_S}{\epsilon} + \frac{\epsilon_i}{\lambda_i \epsilon} \right]^{-1} \quad (11)$$

for the metal-semiconductor contact with both the surface states and the interfacial layer. If $\frac{d\phi_b}{dE}$ is appreciable in comparison with the width of the semiconductor depletion region, the surface states effect cannot be overlooked.

From Eq. (3) we see that m is a characterization parameter for the I-V relation. It is especially meaningful in the forward bias condition with $V > \frac{3kT}{q}$. Since both A^* and ϕ_b are electric field dependent, a small deviation of m from unity should occur and

$$m = \frac{q}{kT} \frac{dV}{d\ln J} = \left[1 - \frac{kT}{2qV_e} \frac{d(\ln A^*)}{d(\ln E)} - \frac{\Delta\phi_b}{4V_e} + \frac{E}{2V_e} \frac{\partial\phi_b}{\partial E} - \frac{\alpha}{2} \frac{E}{V_e} \right]^{-1} \quad (12)$$

In this equation, the contribution due to the second and third terms alone is small. It is shown that m equals 1.04 for the W-GaAs diode.²⁴ From Eq. (11) we can see that if the surface state density D_S is high, $\frac{d\phi_b}{dE} = 0$. A greater deviation of m from unity can only be explained through an adjustable parameter α . The physical origin of α could be the electrostatic dipole or the interfacial layer.²⁹

Since the current transport is not the main subject of this study, no further exploring will be pursued. In Chapter VI we shall present some experimental results to substantiate the points raised in this chapter.

In the following chapter another aspect of the metal-semiconductor contact properties, namely the capacitance and voltage relation, will

be studied in some detail. The effect of deep level impurities on C-V characteristics will also be investigated.

CHAPTER III

THE CAPACITANCE-VOLTAGE CHARACTERISTICS OF SCHOTTKY BARRIER DIODES IN THE PRESENCE OF DEEP LEVEL IMPURITIES

Introduction

In metal-semiconductor contact, the conduction and valence bands of the semiconductor are brought into a definite energy relationship with the Fermi level in the metal. This relationship serves as a boundary condition on the solution of Poisson's equation in the semiconductor.

Using abrupt junction approximation, the following relation is obtained²⁴

$$C^2 = \frac{q\epsilon N_D}{2\left[\phi_b - V - \frac{kT}{q} \left(1 + \ln \frac{N_C}{N_D}\right)\right]} \quad (13)$$

$$= \left[\frac{q\epsilon N_D}{2V_e} \right] \quad (13a)$$

Eq. (13a) can be rewritten in the form

$$\frac{1}{C^2} = \frac{2V_e}{q\epsilon N_D} \quad (14)$$

or

$$N_D = \frac{-2}{q\epsilon} \left(\frac{d(C^{-2})}{dV} \right)^{-1} \quad (15)$$

If the donor concentration N_D is uniformly distributed throughout the semiconductor, then from Eq. (14), the slope of a plot of C^{-2} versus

V for reverse bias yields the donor concentration. The barrier height can be obtained from the extrapolated intercept of the relationship on the voltage axis. If N_D is not a constant spatially, one can still utilize the differential capacitance method to determine the doping profile from Eq. (15). However, the presence of the deep level impurities in GaAs makes it difficult to interpret the measured capacitance. This is due to the fact that the deep impurities do not respond to the high frequency test signals, yet its influence on the diode is observable.^{9,10,11,12} Previous reports deal with the following physical situations at a temperature higher than the freeze-out temperature of the deep impurity states: First of all, the diode is placed at zero bias, such that the deep impurity centers are filled with electrons. After applying reverse bias, the deep impurity centers in the depletion region of the diode start to ionize or deionize. This process, in turn, causes the diode capacitance to vary according to the characteristics of the deep impurities.

Several models have been suggested to describe the situation, but the results are not in good agreement. In the following section, the existing models are reviewed. A model which is originally for deep level impurities in p-n step junction will be discussed in some detail. It shall be proved experimentally in Chapter VI that it applies equally well to the Schottky barrier diode.

Review of the Existing Models

The first detailed treatment of the metal-semiconductor C-V properties was presented by Goodman.⁸ The effects of an insulating interfacial layer between the metal and semiconductor and of traps (deep level impurities) in the depletion region have been evaluated.

Goodman's model was modified by Senechal and Basinski¹¹ by taking into account a more sophisticated charge distribution. Using a simplified energy band diagram (Figs. 2(a) and 2(b)), a small variation in DC voltage is given by

$$\Delta V = \frac{\Delta Q}{C} = \frac{qN_D A \Delta W}{\frac{\epsilon A}{W}} + \frac{qN_T A \Delta W}{\frac{\epsilon A}{(W-\lambda_o)}} \quad (16)$$

This equation can be rearranged as

$$- \left(\frac{\Delta V}{\Delta C^{-2}} \right) = \left(\frac{q\epsilon A^2}{2} \right) \left[(N_D + N_T) - \left(\frac{N_T \lambda_o}{\epsilon A} \right) C \right] \quad (17)$$

where $C = \frac{\epsilon A}{W}$ is the high frequency capacitance. This is Zohta's basic model.¹³ Senechal and Basinski replaced N_T with $N_T[1-\exp(-e_n t)]$ and λ_o with $\lambda(t)$. Their model has the form¹¹

$$- \left(\frac{\Delta C}{\Delta C^{-2}} \right) = \left(\frac{q\epsilon A^2}{2} \right) \left\{ N_D + N_T[1-\exp(-e_n t)] - \left(\frac{\lambda(t)N_T}{\epsilon A} \right) [1-\exp(-e_n t)] C \right\} \quad (18)$$

Experimentally, this is a fairly complicated equation. In order to obtain the value of e_n , several approximations are needed (i.e., $\Delta V = V_2 - V_1$, $C = \frac{2C_1 C_2}{C_1 + C_2}$ and $\Delta C^{-2} = C_2^{-2} - C_1^{-2}$). To obtain the accurate values for ΔV , C and ΔC^{-2} requires small step variation in V . This, in turn, makes capacitance measurement lack necessary accuracy. Nevertheless, from the above C-V experiment, they have determined the energy level for oxygen in n-type GaAs to be 0.9 eV below the conduction band edge. An extension of their theory was derived by Glover¹² to include nonuniform impurity distribution in the semiconductor.

All of the models discussed above have involved capacitance versus time measurement. On the other hand, Zohta¹³ has combined the Senechal-

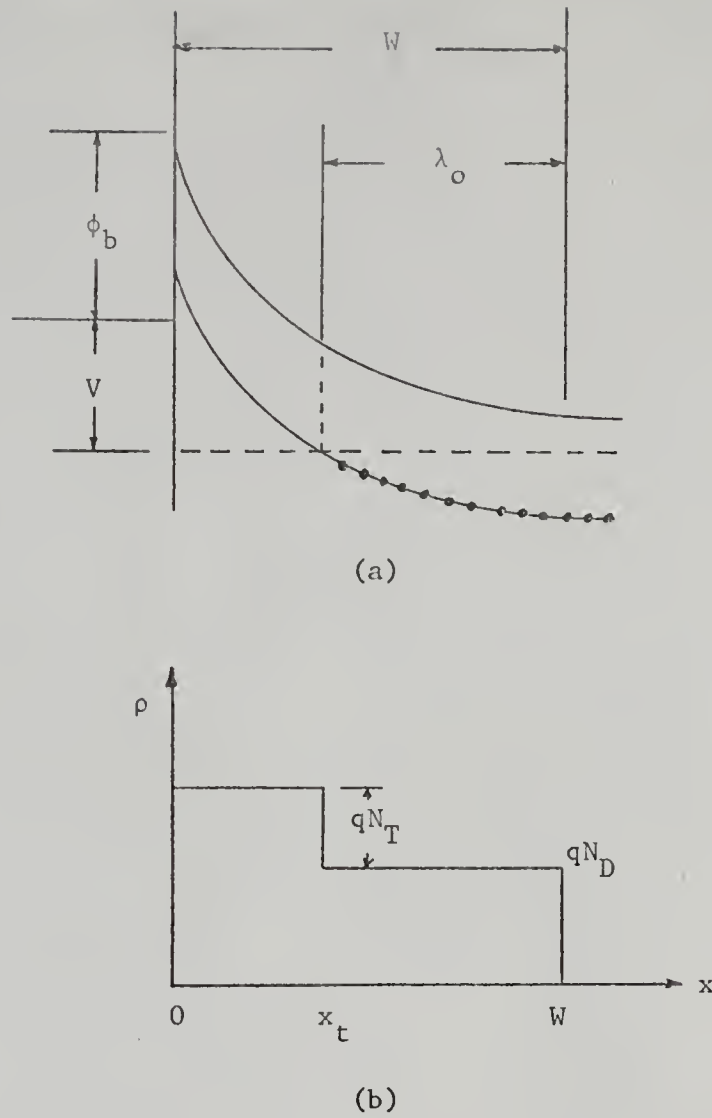


Fig. 2 (a) Energy band diagram of a metal-semiconductor (n-type) in the presence of donor-type deep level impurities
(b) Spatial distribution of charges.

Basinski¹¹ and Copeland's³⁰ models and has been able to derive deep impurity information without resorting to the transient measurement. Their results will be evaluated and compared in a later chapter (see Table 2).

In the following section, by extending the model by Sah et al.¹⁵ on the p-n junction capacitance to the metal-semiconductor Schottky barrier diode capacitance, a straightforward and simple method is presented for determining the deep impurity parameters. In the meantime it is necessary to discuss the electron transport associated with the deep level impurity centers prior to studying a special physical situation.

Transition Processes in Deep Impurity Centers

As first suggested by Williams,⁹ the transient phenomenon in capacitance on the Au-GaAs (n-type) Schottky barrier diode is due to the emptying of the filled deep impurity centers in the depletion region. To facilitate the discussion of the processes involved, the energy band diagram of the semiconductor with single level deep impurity centers is shown in Fig. 3. There are eight possible thermal and optical processes associated with the deep impurity centers and excess carriers.¹⁵ The rate equation is given by

$$\frac{dn_T}{dt} = (c_n n + e_p) p_T - (c_p p + e_n) n_T \quad (19)$$

Here $\frac{dn_T}{dt}$ denotes the rate of change in electron concentrations in the deep impurities. The exact solution for Eq. (19) is complicated and can only be obtained by solving the continuity and rate equations simultaneously.

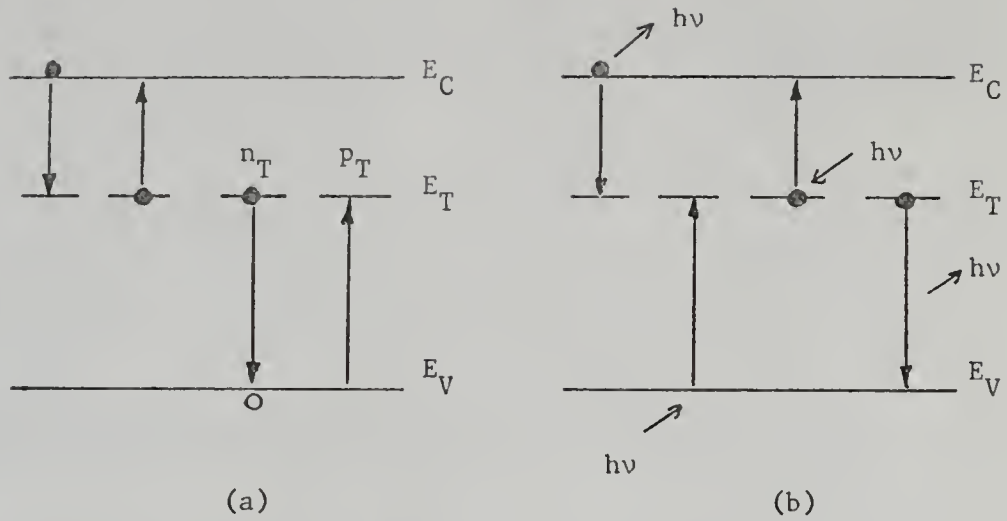


Fig. 3. The energy band diagram and
(a) four thermal and (b) four optical
transition processes between the deep
level impurity and the conduction band.

(After Sah et al., Ref. 15)

However, with the case we are dealing here, a simplification is possible. For the metal-semiconductor Schottky barrier structure, the charge distribution in the depletion region is shown in Fig. 2(b). Charge neutrality is assumed outside of the depletion region $0 < x < w$. This approximation allows the use of constant quasi-Fermi levels in this region. Inside the depletion region, the constant quasi-Fermi level approximation is still adequate, since all that is necessary for simplification is the depletion condition $n = p = 0$. Then the rate equation becomes

$$\frac{dn_T}{dt} = e_p N_T - n_T(e_n + e_p) \quad (19a)$$

Here the totality condition $N_T = n_T + p_T$ is used. The solution of Eq. (19a) subject to the initial condition of $n_T(t=0) = 0$ is

$$n_T(t) = N_T \left[1 - \left\{ \frac{e_p}{(e_n + e_p)} + \left[\frac{e_n}{(e_n + e_p)} \right] \exp[-(e_n + e_p)t] \right\} \right] \quad (20)$$

This time dependence of charge density in the depletion region contributes to the transient phenomenon in the capacitance.

Dark Transient Capacitance

The high frequency capacitance of a Schottky barrier diode is given by

$$C = \frac{dQ(W)}{dV(W)} = \frac{\epsilon A}{W}$$

The main task in deriving the capacitance expression is to obtain the depletion region width W . In the presence of donor-like deep level impurities, the net charge distribution can be approximated by (see Fig. 2(b))

$$\rho(x) = q \left[N_D + \frac{N_T e_n}{(e_n + e_p)} \right] \quad \text{for } 0 < x < x_t \quad (21a)$$

$$\rho(x) = q N_D \quad \text{for } x_t < x < W \quad (21b)$$

and

$$\rho(x) = 0 \quad \text{for } x > W \quad (21c)$$

After solving Poisson's equation, the total depletion layer width is¹⁵

$$W = \left[\frac{(N_T(1-\alpha))}{(N_D + \alpha N_T)} \right] \left[\frac{2\epsilon \phi_t}{q(N_D + N_T)} \right]^{1/2} + \frac{\left\{ (2\epsilon/q) [(N_D + \alpha N_T)(V_{bi} + V_R) + N_T(1-\alpha)\phi_t] \right\}^{1/2}}{(N_D + \alpha N_T)} \quad (22)$$

where

$$\alpha = \frac{e_n}{e_n + e_p} \quad (22a)$$

$$\phi_t = \frac{E_f - E_T}{q} \quad (22b)$$

At large reverse bias voltage, the depletion width becomes

$$W = \left[\frac{2\epsilon (V_{bi} + V_R)}{(N_D + \alpha N_T)} \right]^{1/2} \quad (22c)$$

Then, for an ideal Schottky barrier diode, the high frequency capacitance can be expressed as

$$C = \left[\frac{q\epsilon A^2 (N_D + n_T)}{2(V_{bi} + V_R)} \right]^{1/2} \quad (23)$$

By combining Eqs. (20) and (23), the transient capacitance for the condition of $e_n \gg e_p$ ¹¹ is

$$C(t) = \left\{ \frac{q\epsilon A^2}{2(V_{bi} + V_R)} \left[N_D + N_T(1 - \exp(-e_n t)) \right] \right\}^{1/2} \quad (24)$$

$$= \left\{ \frac{q\epsilon A^2 (N_D + N_T)}{2(V_{bi} + V_R)} \left[1 - \left(\frac{N_T}{N_D + N_T} \right) \exp(-e_n t) \right] \right\}^{1/2} \quad (24a)$$

where V_R is a unit step applied voltage.

The initial capacitance ($t = 0^+$) is

$$C(0^+) = \left[\frac{q\epsilon A^2 N_D}{2(V_{bi} + V_R)} \right]^{1/2} \quad (25)$$

and the final steady-state value is

$$C(t=\infty) = \left[\frac{q\epsilon A^2 (N_D + N_T)}{2(V_{bi} + V_R)} \right]^{1/2} \quad (26)$$

In addition, if the capacitance values are taken at times such that

$$\left(\frac{N_T}{N_D + N_T} \right) \exp(-e_n t) \ll 1$$

then from Eqs. (20) and (24) the time varying capacitance is an exponential function of time:

$$C(t) = \left[\frac{q\epsilon A^2 (N_D + N_T)}{2(V_{bi} + V_R)} \right]^{1/2} \left[1 - \frac{1}{2} \left(\frac{N_T}{N_D + N_T} \right) \exp(-e_n t) \right] \quad (27)$$

From Eqs. (25) and (26), the shallow and deep impurity doping concentrations can be determined, while the transient time constant is obtained from Eq. (27).

The time constant of the transient capacitance gives us the value of the thermal emission rate of electrons from the deep impurities. It is worth noting that the thermal emission rate is not an equilibrium value. Under the influence of an electric field, the impurity potential barrier is lowered by an amount ΔE . Thus the thermal emission rate is given by³¹

$$e_n(E) = e_n(0) \exp[\Delta E/kT] \quad (28)$$

where

$$e_n(0) = (N_C v_t S_n) \exp\left(-\frac{E_C - E_T}{kT}\right) \quad (29)$$

and the statistical weighting factor has been assumed to be unity. If the emission rate is independent of the electric field, the activation energy of the deep impurity states can be obtained through the measurement of the temperature dependence of the emission rate by using Eq. (29). The transient capacitance of Eq. (27) would also show true exponential dependence on time and the electron capture cross section S_n can also be calculated from Eq. (29).

For the case of acceptor-type deep level impurities, the time dependence of the capacitance can be expressed as

$$C(t) = \left\{ \frac{q\epsilon A^2}{2(V_{bi} + V_R)} [N_D - N_T \exp(-e_n t)] \right\}^{1/2} \quad (30)$$

Again, the values of N_D , N_T and e_n can be determined by Eq. (30) from the measurements of time constant, the initial and final values of capacitance.

Transient Photocapacitance

In the dark transient capacitance measurement, the deep donor impurity centers were filled with electrons initially at zero bias condition. The filling of electrons at the deep impurity centers can also be achieved by shining the interband light ($h\nu > E_g$) onto the top surface of the device which is reverse biased at a certain voltage. Upon reaching the steady state, the recapture of photoinjected electrons by the deep impurities in the depletion region is balanced by the thermal release of electrons from the impurities. When the light is removed, the thermal release of the remaining captured electrons from the deep impurities causes the change in the diode capacitance.

From the time constant of this transient capacitance measurement, the thermal emission rate can be obtained.

Summary

We have demonstrated in this chapter that some parameters of the deep level impurity can be obtained by using transient capacitance measurement. These parameters are important to the kinetic behavior of excess carriers. For example, if there is only one electrically active impurity level, the lifetime of holes in low level injection in an n-type semiconductor is

$$\tau_p = \frac{1}{v_t S_p N_T} \quad (31)$$

Here the values of S_p and N_T are determined by the transient capacitance measurement. In the next chapter, the behavior of excess carriers in a semiconductor with the presence of deep impurity centers will be examined.

CHAPTER IV
RECOMBINATION AND TRAPPING PROCESSES
IN BULK n-TYPE GaAs IN THE PRESENCE
OF DEEP LEVEL IMPURITIES

Introduction

In the previous chapter, the properties of deep level impurities in a semiconductor are studied in terms of its thermal activation energy, electron emission rate and capture cross section through C-V relationship in a Schottky diode. However, the deep impurity can also serve as a trapping or recombination center for excess carriers in the semiconductor.³² A complete review of the effects of trapping on carrier transport is done by van Roosbroeck,³³ while Shockley-Read³² and Sah-Shockley³⁴ models provide the necessary trapping and recombination statistics. In the case of the deep impurity not being an effective recombination center, Hall's band to band radiative recombination model³⁵ is applicable.

The most effective method for studying the trapping and the recombination mechanisms is the carrier lifetime measurement. We choose the photomagnetoelectric (PME) and the photoconductive (PC) effects to measure the carrier lifetimes, and investigate the effects of chromium and oxygen on the transport of excess carriers in bulk n-type GaAs.

In this chapter, a generalized theory to account for the observed PME and PC effects on chromium and oxygen doped GaAs is developed by

considering the carrier lifetimes as a function of the injection and the effect of trapping. Based on this theory, we are able to determine the properties of chromium and oxygen as recombination and trapping centers.

Charge Neutrality in Semiconductors

In steady state injection, the emission and capture of carriers by the impurity centers cause the charge in such centers to change from its equilibrium values. Utilizing the energy band diagram for an n-type semiconductor with one shallow level donor and one deep level acceptor impurities shown in Fig. 4, the requirement of charge neutrality gives

$$p + (N_D - n_D) - N_T^- - n = 0 \quad (32)$$

By subtracting the thermal equilibrium contribution we have

$$\Delta p = \Delta n + \Delta n_D + \Delta N_T^- \quad (33)$$

Applying Sah-Shockley statistics³⁴ to this physical situation we obtain

$$N_T^- = N_T^0 \frac{(n+n_1)c_n^0}{(p+p_1)c_p^-} \quad (34)$$

and

$$N_T = N_T^- + N_T^0 \quad (34a)$$

Consider the case of undercompensation ($N_D > N_T$) at temperatures low enough that the semiconductor is an extrinsic n-type. The quantities n_1 , p_1 and p_o are negligible and the statistics give³⁶

$$n_D = \frac{N_T}{N_D - N_T} n_o \quad (35)$$

Also from Eqs. (34) and (34a) we obtain

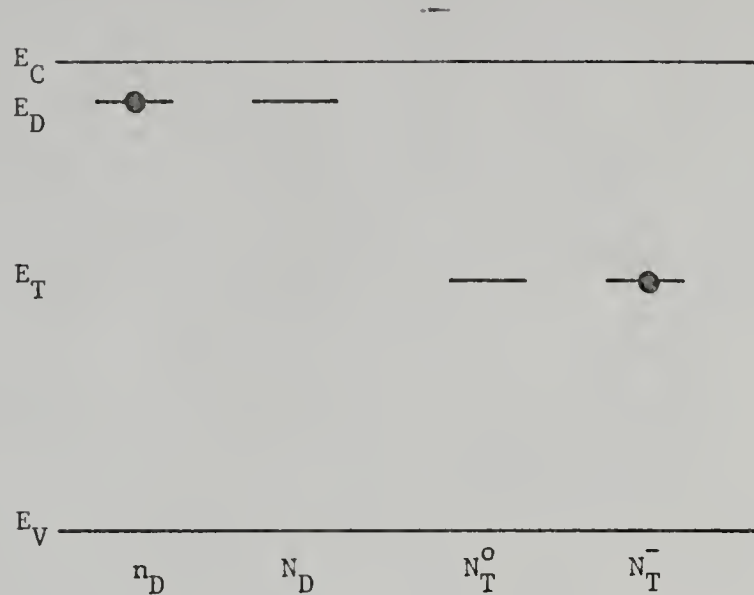


Fig. 4 Localized states introduced by the shallow and deep level impurities in the forbidden band for a semiconductor. The centers are shown in their available charge states.

$$N_T^O = N_T \frac{\Delta p}{\Delta p + n\gamma} \quad (36)$$

where

$$\gamma = \frac{c_n^O}{c_p}$$

Realizing that in thermal equilibrium

$$(N_D - n_D)_{\text{th. eq.}} = N_T + n_D \cong N_T \quad (37)$$

and

$$(N_T^-)_{\text{th. eq.}} = N_T \quad (38)$$

the charge neutrality equation (Eq.(33)) can be rewritten as

$$\Delta p + \frac{\Delta p N_T}{\Delta p + n\gamma} = \Delta n + \Delta n N_T \left(\frac{N_D}{N_D - N_T} n_O + \Delta n \right)^{-1} \quad (39)$$

Therefore, the density of carriers trapped in the impurity states is a function of the injected carrier densities. If the density of these traps is larger than the excess carrier density, the charge in them will play an important role in preserving the charge neutrality under the steady state injection. This has been shown by Agraz and Li.^{37,38} In a certain injection range we can define the parameters Γ and ℓ such that

$$\Delta p = \Gamma \Delta n^\ell \quad (40)$$

where $\Gamma = \frac{\tau_p}{\tau_n} < 1$ for hole trapping.

Trapping and Recombination Processes Through Deep Level Impurities

In order to understand the charge states in the acceptor levels under dark and illumination conditions, an energy band diagram for the n-type semiconductor is presented in Fig. 5. In thermal equilibrium,

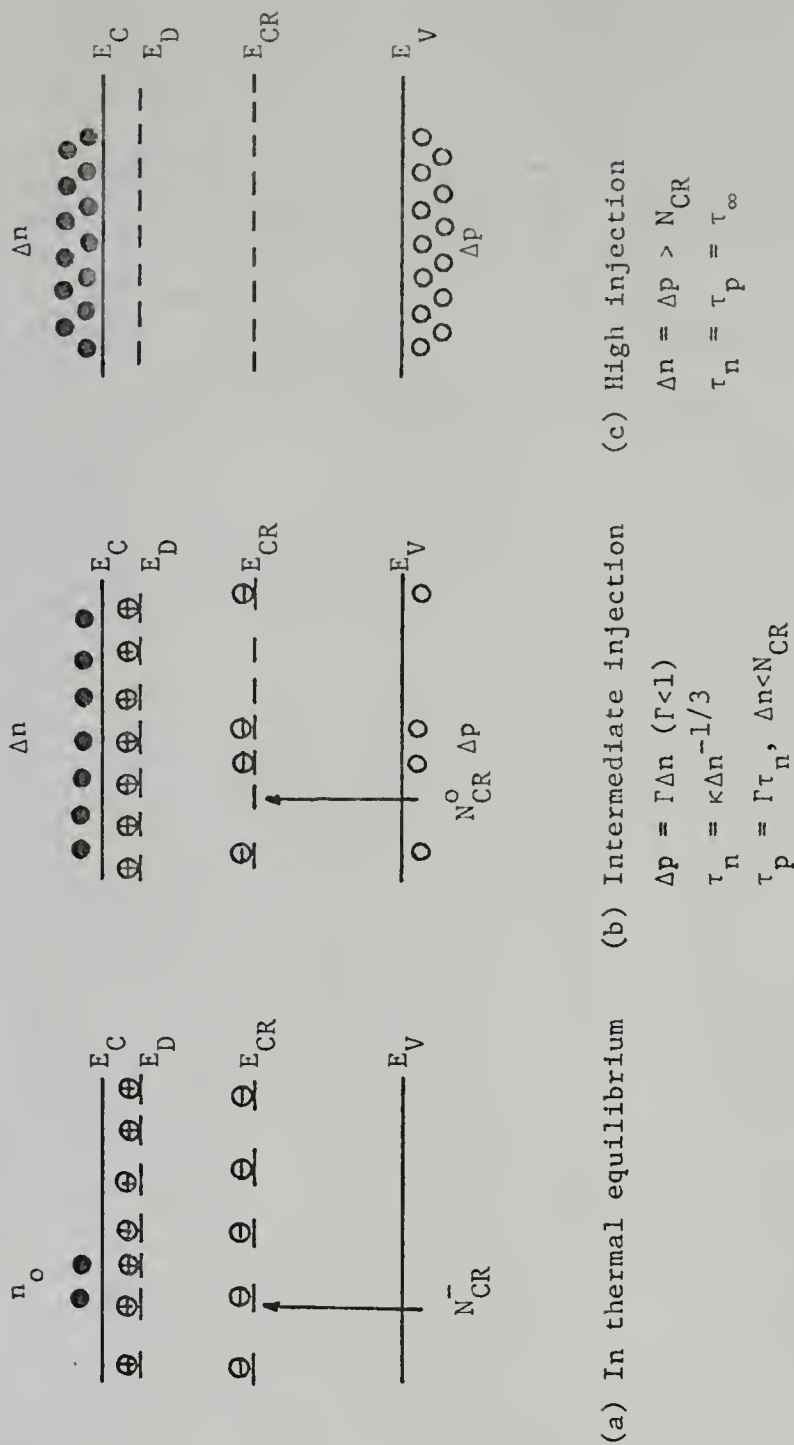


Fig. 5 Energy band diagram for a semiconductor doped with deep level acceptor impurities in thermal equilibrium and under steady state injection:
(a) thermal equilibrium; (b) intermediate injection; (c) high injection.

the acceptor levels are occupied by the conduction electrons (see Fig. 5(a)) and are in negative charge state. For steady-state injection, the free holes in the valence band are captured by the negatively charged acceptor centers due to the Coulomb attractive potential. As a result, these trapped holes will tend to destroy the charge balance in the localized and band states. This is true for the case when the acceptor density is much higher than the thermal equilibrium electron concentration. The impurity centers tend to serve as recombination centers.

The recombination rate is³⁴

$$\begin{aligned}
 R &= (np - n_i^2) \frac{N_T c_n^0 c_p^-}{c_n^0 (n + n_1) + c_p^- (p + p_1)} \\
 &\approx (n_0 \Delta p + p_0 \Delta n) \frac{N_T c_n^0}{n\gamma + \Delta p} \\
 \frac{\Delta}{\tau_n} \frac{\Delta n}{\tau_p} &= \frac{\Delta p}{\tau_p} \quad (41)
 \end{aligned}$$

The carrier lifetimes depend on the injected carrier density as we have seen in the above equation. This dependence can be expressed in terms of a power-law relationship between τ_n and Δn , that is

$$\tau_n = \kappa \Delta n^\beta \quad (42)$$

in certain injection ranges. In the high injection region, the charge states in localized and band states are essentially controlled by the injected carrier densities. The electron and hole lifetimes are equal and independent of injection. The trapping constant Γ is equal to unity and $\beta = 0$. In other injection ranges, it is still possible to have $\beta = 0$, although it usually assumes values other than zero.^{37,38}

Radiative Recombination in the Host Crystal

If the semiconductor is heavily doped or if the deep level impurities in a semiconductor are in a neutral charge state, the recombination mechanism is most likely to be the band to band radiative recombination. In a nondegenerate semiconductor, the rate at which excess electrons and holes disappear is proportional to the product of the electron and hole concentrations. Thus the recombination rate is

$$R = B_r (np - n_i^2) \quad (43)$$

For large injection, $\Delta n \gg n_o$, $\Delta p \gg p_o$,

$$R \approx B_r \Delta n \Delta p \quad (44)$$

The capture probability B_r can be evaluated theoretically by setting the equilibrium rate of radiative recombination equal to the total amount of black-body radiation absorbed by the crystal due to band to band process. It has been derived by Hall³⁵ and is given by

$$B_r = 0.58 \times 10^{-12} \sqrt{\epsilon} \left(\frac{m_o}{m_e + m_h} \right)^{3/2} \left(1 + \frac{m_o}{m_e} + \frac{m_o}{m_h} \right) \left(\frac{300}{T} \right)^{3/2} E_g^2 \quad (45)$$

The band to band radiative carrier lifetimes for large injection are defined in terms of the recombination rate

$$R = \frac{\Delta n}{\tau_n} = \frac{\Delta p}{\tau_p} \quad (46)$$

and are

$$\tau_n = \tau_p = \frac{1}{B_r \Delta n} = \frac{1}{B_r \Delta p} \quad (47)$$

It is noted here that internal absorption will increase the apparent radiative lifetime in samples which are thick compared to the absorption distance for the recombination radiation. Equations (46) and (47) also

indicate that the capture probability B_r can be determined at various temperatures by measuring carrier lifetimes at certain injection ranges. In the following section, the method for obtaining the quantities τ_n , τ_p , B_r and Δn will be presented.

Carrier Lifetime Measurement Using PME and PC Effects

The theory for the PME effect involves the solution of the continuity equation for the carriers injected at the illuminated surface. Detailed descriptions of the physical system have been given by van Roosbroeck³³ and Agraz and Li.³⁷ In this section, we shall present a generalized theory to account for the trapping effect in the presence of deep level impurities in bulk semiconductors.

With the help of Eqs. (40) and (42), the generalized expressions for PME short-circuit current and photoconductance can be derived as follows: The photoconductance per unit sample length-to-width ratio is given by

$$\begin{aligned}\Delta G &= q \int_0^d (\mu_n \Delta n + \mu_p \Delta p) dy \\ &= q \mu_n \int_0^{\Delta n_0} (\Delta n + \frac{\Delta p}{b}) \frac{D_a d(\Delta n)}{(2 \int_0^{\Delta n} D_a R d(\Delta n))^{\frac{1}{2}}} \end{aligned} \quad (48)$$

where $D_a = \frac{2D_n \Gamma}{\Gamma+b}$ is the effective diffusion constant and

$$R = (\frac{1}{\kappa}) \Delta n^{1-\beta} \quad (48a)$$

We obtain the general expression for photoconductance ΔG by solving Eqs. (48) and (48a).

$$\Delta G = [\frac{2q\mu_n}{(\ell+\beta+1)}] [(1+\ell-\beta)D_p \Gamma \kappa]^{\frac{1}{2}} \Delta n_0^{\frac{\ell+\beta+1}{2}} \quad (49)$$

The PME short-circuit current per unit width I_{PME} is

$$I_{PME} = q\mu_p (1+b)B \int_0^{\Delta n_0} D_a d(\Delta n) \quad (50)$$

$$= 2q\mu_p (1+b)D_p \Gamma B \Delta n_0^\ell \quad (51)$$

The relationship between I_{PME} and ΔG can now be derived from Eqs. (49) and (51) by eliminating Δn_0 from these two equations. The result yields

$$I_{PME} = 2q\mu_p (1+b)B\Gamma D_p \left[\frac{(1+\ell+\beta)^2}{4(1+\ell-\beta)D_p \Gamma \kappa} \right]^{\frac{1}{\ell+\beta+1}} \left(\frac{\Delta G}{q\mu_n} \right)^{\frac{2}{\ell+\beta+1}} \quad (52)$$

This general expression of I_{PME} versus ΔG is rather important since it provides a direct correlation among the measureable quantities I_{PME} , μ_n , B and ΔG , and allows us to make a direct comparison of the theoretical prediction with the experimental results.

In general, the electron and hole lifetimes are functions of injection. In order to determine the lifetimes as functions of injection, it is necessary to define an apparent lifetime τ_a in the I_{PME} expression. This can be achieved by rewriting Eq. (52) into

$$I_{PME} = \left(\frac{D_a}{\tau_a} \right)^{1/2} B \Delta G \quad (53)$$

where

$$\tau_a = \frac{1}{2D_p \Gamma^2} \cdot \left[\frac{(1+\ell+\beta)^2}{4(1+\ell-\beta)D_p \Gamma \kappa} \right]^{\frac{-2}{1+\ell+\beta}} \left(\frac{\Delta G}{q\mu_n} \right)^{\frac{2(\ell+\beta-1)}{(\ell+\beta+1)}} \quad (54)$$

is the PME apparent lifetime.

To deduce the electron and hole lifetimes from the PME apparent lifetimes, we make use of the following relation in the presence of trapping³⁹

$$\tau_a = \frac{\tau_n \Delta p + \tau_p \Delta n}{\Delta n + \Delta p} = \frac{\tau_p + \Gamma \tau_n}{1 + \Gamma} = 2\tau_p \quad (55)$$

where we assume $\Gamma = \frac{\tau_p}{\tau_n} < 1$.

In essence, τ_a is a parallel sum of τ_n and τ_p , and is controlled by the shorter of the two lifetimes. Subsequently, the remainder of the parameters Γ and κ can be deduced by using Eqs. (49), (53) and (54).

Since we have made use of Eq. (40), we are assuming that the Shockley-Read type recombination mechanism is dominant; however, the generalized theory is equally applicable to the case of band to band radiative recombination processes. In this particular situation, by setting $\Gamma = 1$ (i.e. $\tau_n = \tau_p$, no trapping), $\kappa = B_r^{-1}$ and $\beta = -1$ in Eq. (52), we obtain an expression for the PME short-circuit current for the radiative recombination. It can be written as

$$I_{PME} = \frac{B}{6} \left(\frac{B_r}{q\mu_n} \right) \Delta G^2 \quad (56)$$

where the electron and hole mobility ratio b is assumed to be much greater than unity. Comparing this equation with Eq. (53) we obtain the electron and hole lifetimes for band to band radiative recombination

$$\tau_n = \tau_p = 72D_p \left(\frac{q\mu_n}{B_r \Delta G} \right)^2 \quad (57)$$

This equation shows that the electron and hole lifetimes are inversely proportional to the square of the photoconductance under a large injection condition.

We can also rewrite Eq. (56) into

$$B_r = \frac{6(q\mu_n)}{(\Delta G)^2} \left(\frac{I_{PME}}{B} \right) \quad (58)$$

This equation provides a simple method for determining the capture probability B_r which is obtained by the concurrent measurements of I_{PME}/B , ΔG and the photo-Hall mobility μ_n .

Summary

After considering the charge neutrality condition in the semiconductor, a simple power-law relation between Δn and Δp is established. By taking into account the variation of carrier lifetimes with injected carrier density and the effect of trapping, a generalized theory for the PME and PC effects is then developed. For acceptor-type deep level impurities in the n-type semiconductor, the Shockley-Read type recombination model is used to interpret the recombination process. On the other hand, Hall's band to band radiative recombination model is used for the semiconductor in the presence of neutral deep impurity centers.

CHAPTER V

EXPERIMENTS

Preparation of Devices

GaAs wafers were n-type oxygen- or chromium-doped single crystals with faces in the (111) plane. The samples were mechanically lapped and chemically etched in a solution of 3:1:1:H₂SO₄:H₂O₂:H₂O at 90°C. Ohmic contacts were provided on the rear surface by evaporation of indium, and alloying at 375°C in a hydrogen atmosphere. The front face was chemically polished prior to evaporation of a gold dot in an area of approximately 3 mm². The gold evaporation was performed in a vacuum with the background pressure of $\sim 5 \times 10^{-8}$ torr.

The packaging of the device was made by using a TO-18 transistor header. By applying silver paste, the ohmic contact side of the diode was "glued" onto the header (collector terminal). After gold wire connections were made, the diodes were baked at 110°C for 24 hours. The basic physical parameters of typical devices fabricated are summarized in Table 1.

Sample Preparation

Two slices of rectangular bar cut from a Cr-doped semi-insulating n-type GaAs single crystal wafer (total chromium impurity density is $1\text{--}3 \times 10^{17} \text{ cm}^{-3}$) were made by the zone-melting method. The sample dimensions are $0.5 \times 1 \times 0.1 \text{ cm}^3$ for Sample No. 1 (S-1) and $0.4 \times 0.8 \times 0.1 \text{ cm}^3$ for

Table 1: Basic Physical Parameters of Typical Au-GaAs
(n-type) Schottky Barrier Diodes at 300°K

* Obtained by Hall-Effect Measurements
** Determined by C-V measurements

Device No.	Dopant n-type GaAs	Resistivity of Bulk GaAs Ω -cm	Area (mm ²)	Carrier * Concentration (cm ⁻³)	Impurity ** Concentration (cm ⁻³)
7	Oxygen	1.65	3.1	$N_D = 1.1 \times 10^{15}$	$N_D = 9.2 \times 10^{14}$
11	Oxygen	0.9	3	$N_D = 1.2 \times 10^{15}$	$N_D = 2.64 \times 10^{15}$
17	Chromium	5.9	3	$N_D - N_T = 6.8 \times 10^{14}$	$N_D - N_T = 5.2 \times 10^{14}$

Sample No. 2 (S-2). A third slice was cut from an oxygen-doped semi-conducting n-type GaAs single crystal ($n \approx 10^{15} \text{ cm}^{-3}$). The dimension for this sample (S-3) is $0.38 \times 0.8 \times 0.04 \text{ cm}^3$. The samples were mechanically lapped with silicon carbide powder on all six faces and chemically etched on the illuminated surface by using a solution of $3 \text{ H}_2\text{SO}_4 : \text{H}_2\text{O}_2 : \text{H}_2\text{O}$. Ohmic contact was made by indium alloying in hydrogen atmosphere at 375°C .

Current-Voltage Measurement

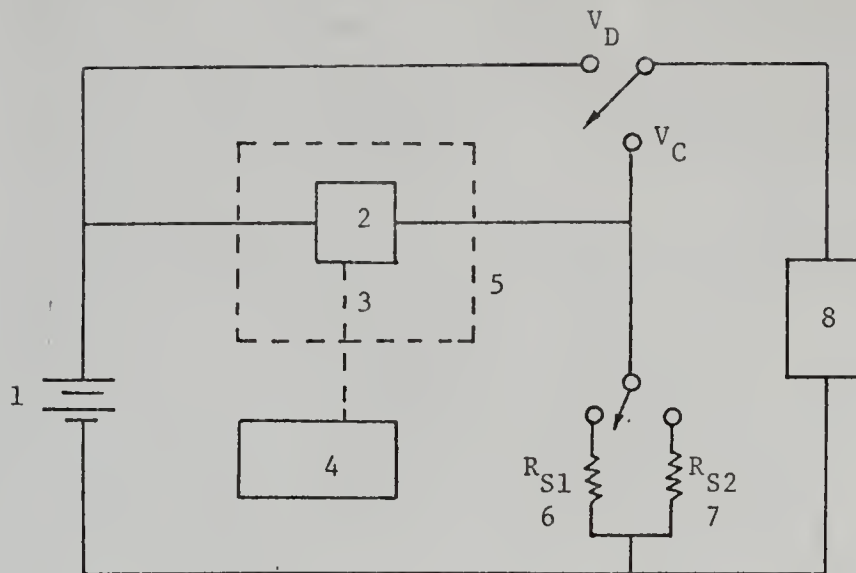
The experimental arrangement for I-V measurements is shown in Fig. 6. The device impedance r_D is always greater than the precision resistors r_{s_1} and r_{s_2} . The input impedance of the digital voltmeter is much greater than r_{s_1} and r_{s_2} also. The current flowing through the diode can be calculated by V_C / r_{s_i} ($i = 1, 2$). The voltage across the diode is obtained by $V_D - V_C$.

Capacitance-Voltage Measurement

A system for measuring the transient capacitance and transient photocapacitance was set up as shown in Fig. 7. It consists of a Wayne-Kerr B641 Capacitance Bridge, a low noise amplifier, a wave analyzer, a Perkin-Elmer 98 Monochromator and an X-Y recorder. The system is calibrated such that the deviation from the balanced value of the capacitance bridge, $\Delta C = C(t) - C(t=\infty)$, is linearly proportional to the DC output of the wave analyzer.

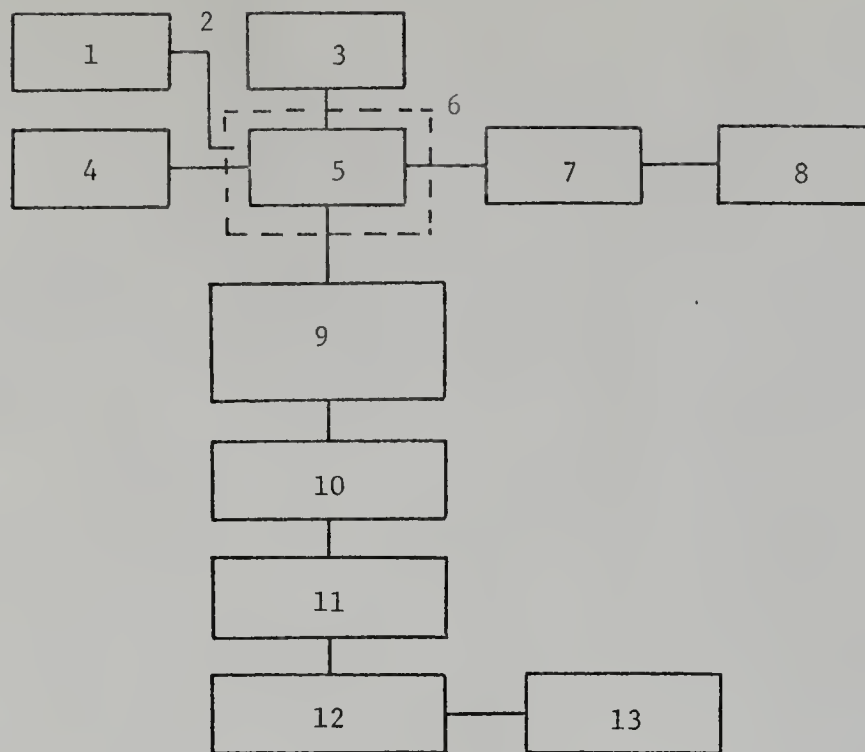
The transient capacitance measurement procedure is as follows:

- (1) At a certain reverse bias voltage, after the steady state is reached, apply a small signal ($< 10 \text{ mV}$) at 100 KHz to null the bridge.



- | | |
|--|--|
| 1. Power Supply | 2. Device |
| 3. Thermocouple | 4. Null Voltmeter |
| 5. Temperature Chamber | 6. Precision Resistor
($10^3 \Omega \pm 1\%$) |
| 7. Precision Resistor
($10^6 \Omega \pm 1\%$) | 8. Digital Voltmeter |

Fig. 6 Test set-up for measuring Schottky barrier diode voltage-current characteristics.



- | | |
|-----------------------|--------------------------|
| 1. Null Voltmeter | 2. Thermo-couple |
| 3. Biasing Circuit | 4. He-Ne Laser |
| 5. Device | 6. Temperature Chamber |
| 7. Monochromator | 8. Tungsten Light Source |
| 9. Capacitance Bridge | 10. Low Noise Amplifier |
| 11. Amplifier | 12. Wave Analyzer |
| 13. X-Y Recorder | |

Fig. 7 Experimental set-up for measuring transient dark and photocapacitance of the metal-GaAs Schottky barrier diodes.

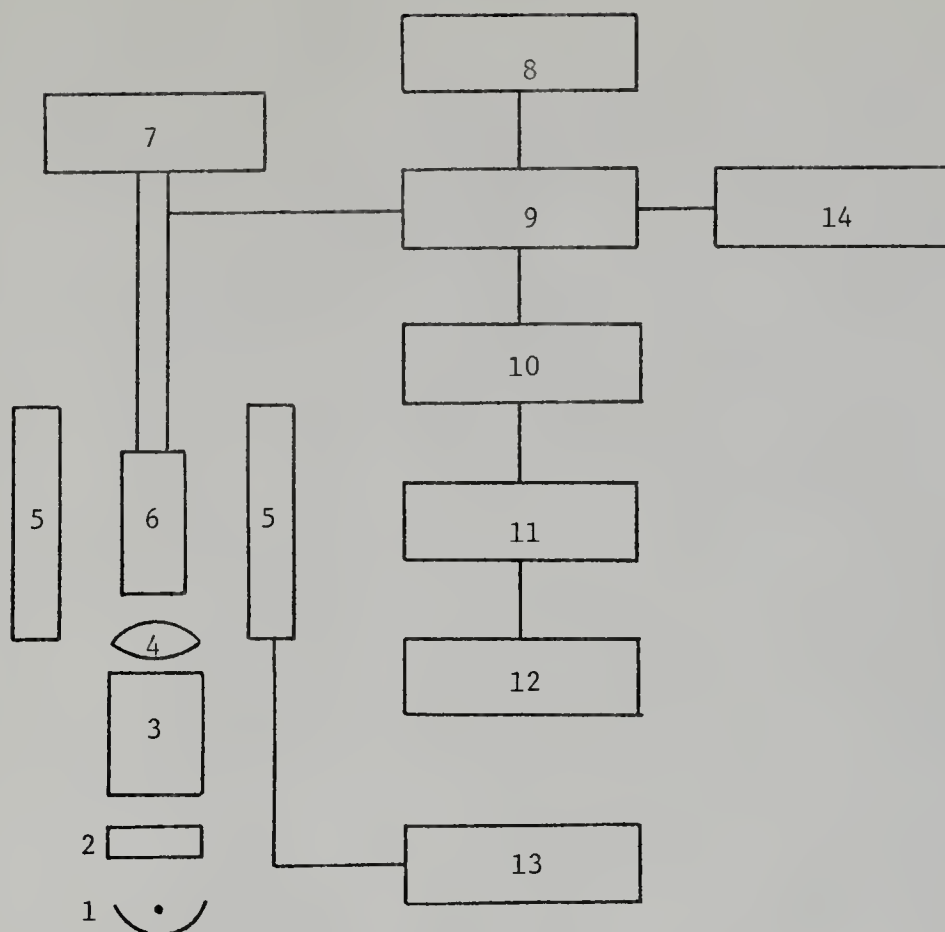
- (2) Leaving the bridge as it is, remove the bias voltage (so that the diode is at zero bias). The null detector has maximum deflection.
- (3) After waiting for 10 minutes, the same reverse bias is suddenly applied to the diode. The bridge is restored to the balance position gradually, and the behavior of restoration is recorded on an X-Y recorder.
- (4) The data are then analyzed according to Eqs. (24) and (30).

Photocapacitance Measurement

The system and procedures for measuring transient photocapacitance are essentially the same as those used for measuring the C-V relationship. The light source is the He-Ne laser with a wavelength of 6328\AA . In steps (2) and (3) above, the removing and applying bias voltages are replaced by shining the light on the diode and removing the light from the diode respectively. The rest of the steps are the same.

Bulk Effect Measurements

The resistivity, Hall-effect and Photo-Hall-effect measurements were performed by using the standard DC method. The measurements were made at 300 and 80°K for S-1 and S-2, at 20.8 and 4.2°K for S-3. The technique for measuring the PME and PC responses using the DC method is described in detail by Li.⁴⁰ For the case of small injection, an AC system was set up. The system assembly is illustrated in Fig. 8. First of all, the system was calibrated such that the DC output of the wave analyzer is linearly proportional to the signal. The tungsten light source was chopped at 400 Hz and the PME and PC signals picked up from the sample were passed through the amplifier and a wave analyzer. The system provides a maximum voltage gain of 10^5 , which allows us to



- | | |
|--------------------------------|--------------------------------|
| 1. Light Source | 8. Constant Current Supply |
| 2. Light Chopping Mechanism | 9. Control Panel |
| 3. Water filter | 10. Low Noise Amplifier |
| 4. Focusing Lens | 11. Wave Analyzer |
| 5. Electromagnet | 12. DC voltmeter |
| 6. Sample | 13. Electromagnet Power Supply |
| 7. "Cryo-Tip" Cryogenic System | 14. Potentiometer |

Fig. 8 Experimental set-up for the AC PME measurement.

measure a relatively small signal. The smallest signal current detected is in the magnitude of 10^{-10} amp, and the signal-to-noise ratio is better than 10.

CHAPTER VI
EXPERIMENTAL RESULTS AND ANALYSES

Introduction

The temperature dependence of Au-GaAs (n-type) Schottky diodes forward I-V characteristics was measured. Values of the barrier height were deduced from these measurements. The reverse I-V measurement was used to study the effect of the interfacial layer.

The transient capacitance measurements of the Schottky diodes were performed between 285 and 316°K. From the temperature dependence of the time constant, the thermal activation energies of the deep level impurities such as oxygen and chromium in n-type GaAs were determined. The capture cross sections for electrons were also calculated from the time constant data.

The bulk effect measurements were performed to obtain the functional dependence of carrier lifetimes on the excess carrier injection. The recombination mechanisms of excess carriers in n-type GaAs with the presence of deep impurities were investigated.

Forward Current-Voltage Measurement of Au-GaAs Schottky Diodes

The forward I-V relation of a Schottky diode by thermionic emission theory for $V > \frac{3kT}{q}$ is

$$J = A^*T^2 \exp \left[\frac{q}{kT} (-\phi_{bo} + \left(\frac{qE}{4\pi\epsilon} \right)^{1/2} + \alpha E \right] \exp \left(\frac{qV}{mkT} \right) \quad (59)$$

The I-V plots for devices D-11 and D-17 at different temperatures are shown in Figs. 9 and 10 respectively. From the slope of these lines, the values of m are calculated through the equation

$$m = \frac{q}{kT} \frac{dV}{d(\ln J)} \quad (60)$$

which are included in Figs. 9 and 10. The appreciable deviation of m values from unity could be caused either by the electro-static dipole or the voltage dividing nature of the interfacial layer; however, the exact cause for this nonideal result still cannot be determined.

Now, if we extrapolate the $\ln I$ versus V plots to the small voltage region till they intercept the $V=0$ ordinate as shown in Figs. 9 and 10, we can obtain the saturation current I_{sat} (see Eq. (7)). In Fig. 11, $\ln (I_{\text{sat}}/T^2)$ versus $10^3/T$ for D-11 and D-17 is illustrated. The slope of these plots yields the barrier height ϕ_b . The values of the barrier height are 0.87 eV and 0.86 eV for D-11 and D-17 respectively. The results indicate that the different deep impurities in n-type GaAs have no effects on the values of the barrier height. These values are within the difference of gold work function ϕ_m and electron affinity of GaAs χ . It is known that²⁴

$$\begin{aligned} \phi_m &= 4.7 \sim 5.2 \text{ eV for Au} \\ \chi &= 4.07 \text{ eV for GaAs} \end{aligned}$$

and thus

$$\phi_{bo} = \phi_m - \chi = 0.63 \sim 1.13 \text{ eV}$$

The reported barrier height for Au-GaAs (n-type) Schottky diodes is 0.90 eV.

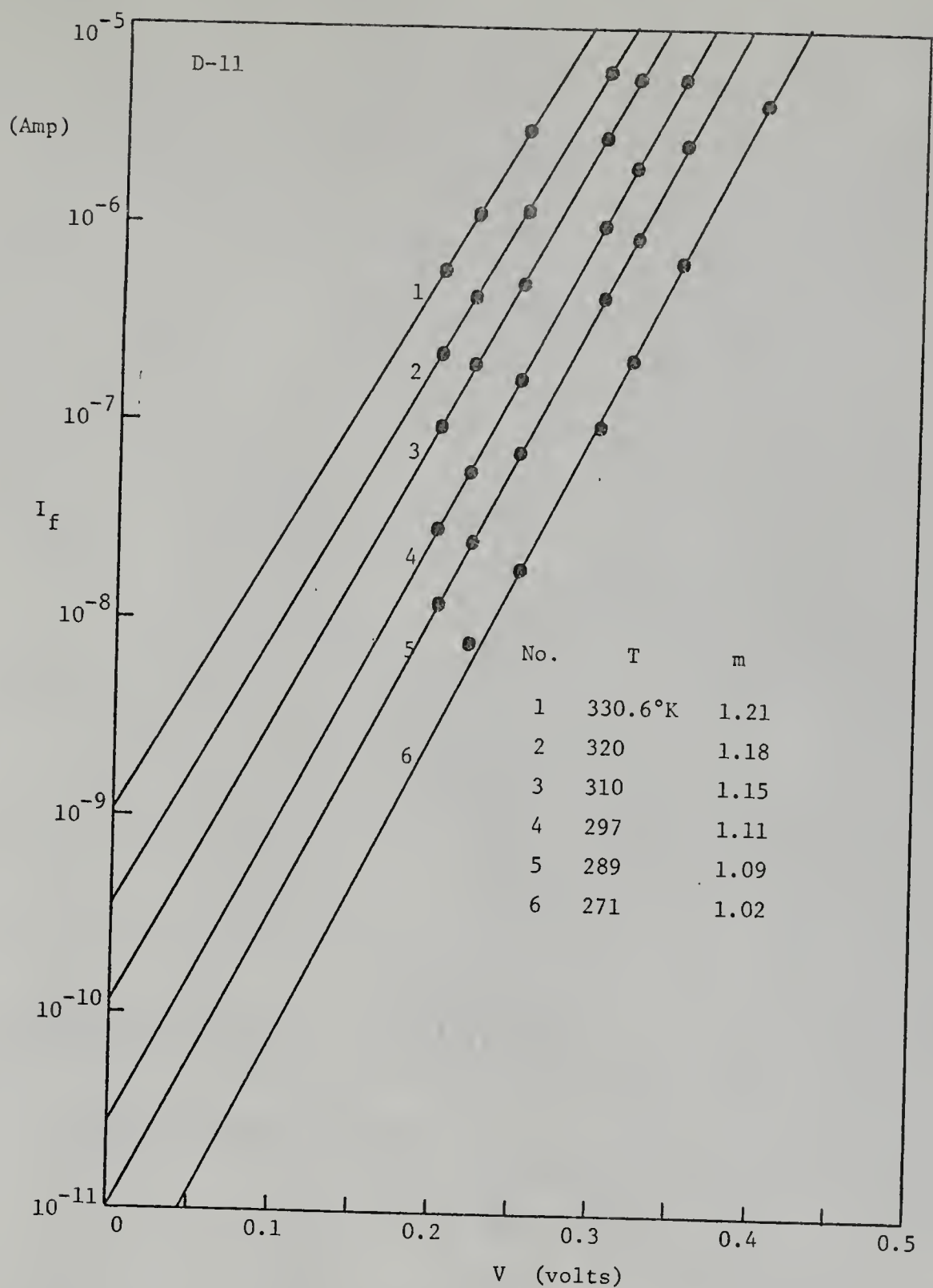


Fig. 9 Forward voltage-current relationship of Au-GaAs (n-type) Schottky barrier diode D-11 at various temperatures.

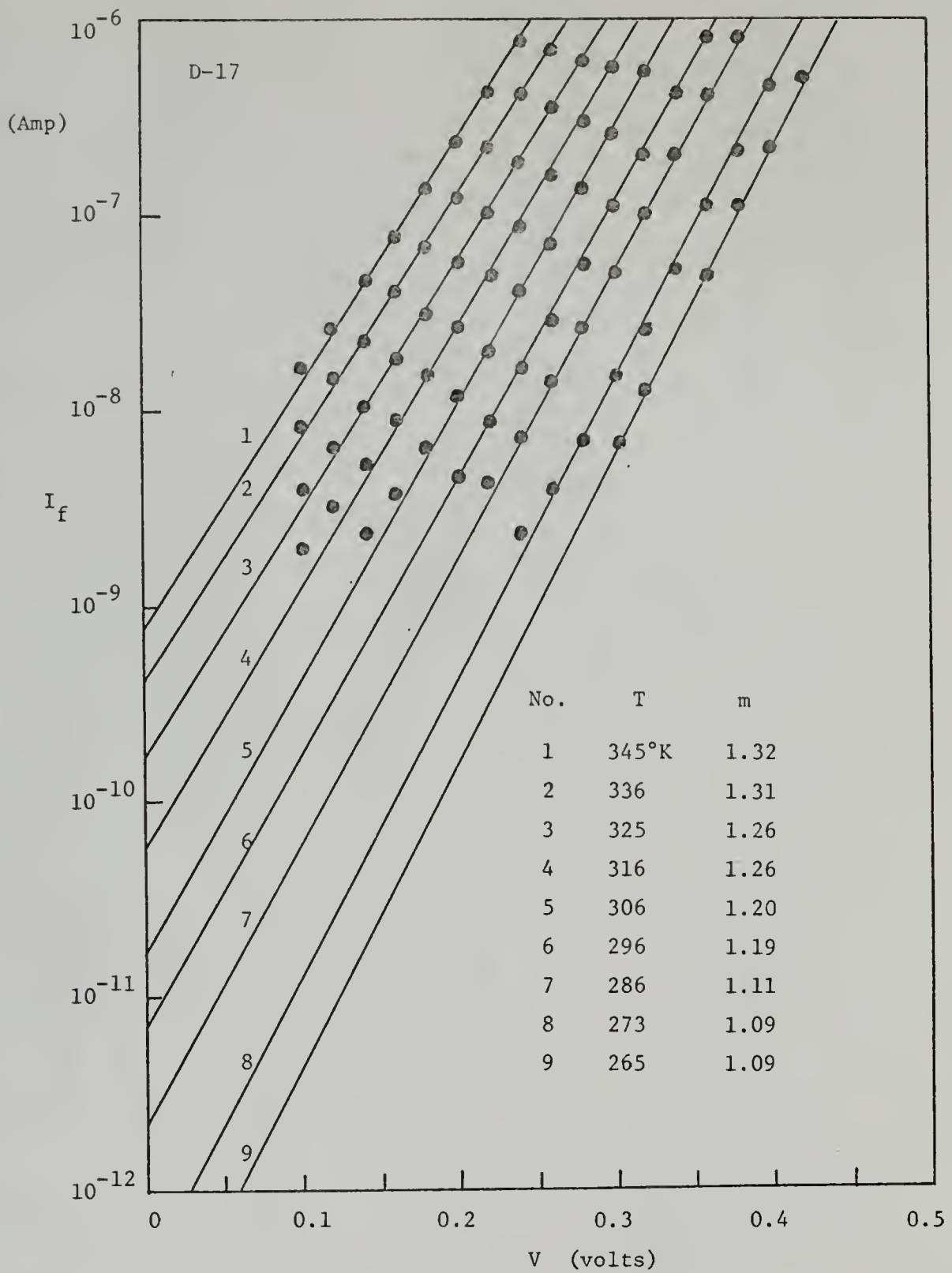


Fig. 10 Forward voltage-current relationship of Au-GaAs (n-type) Schottky barrier diode D-17 at various temperatures.

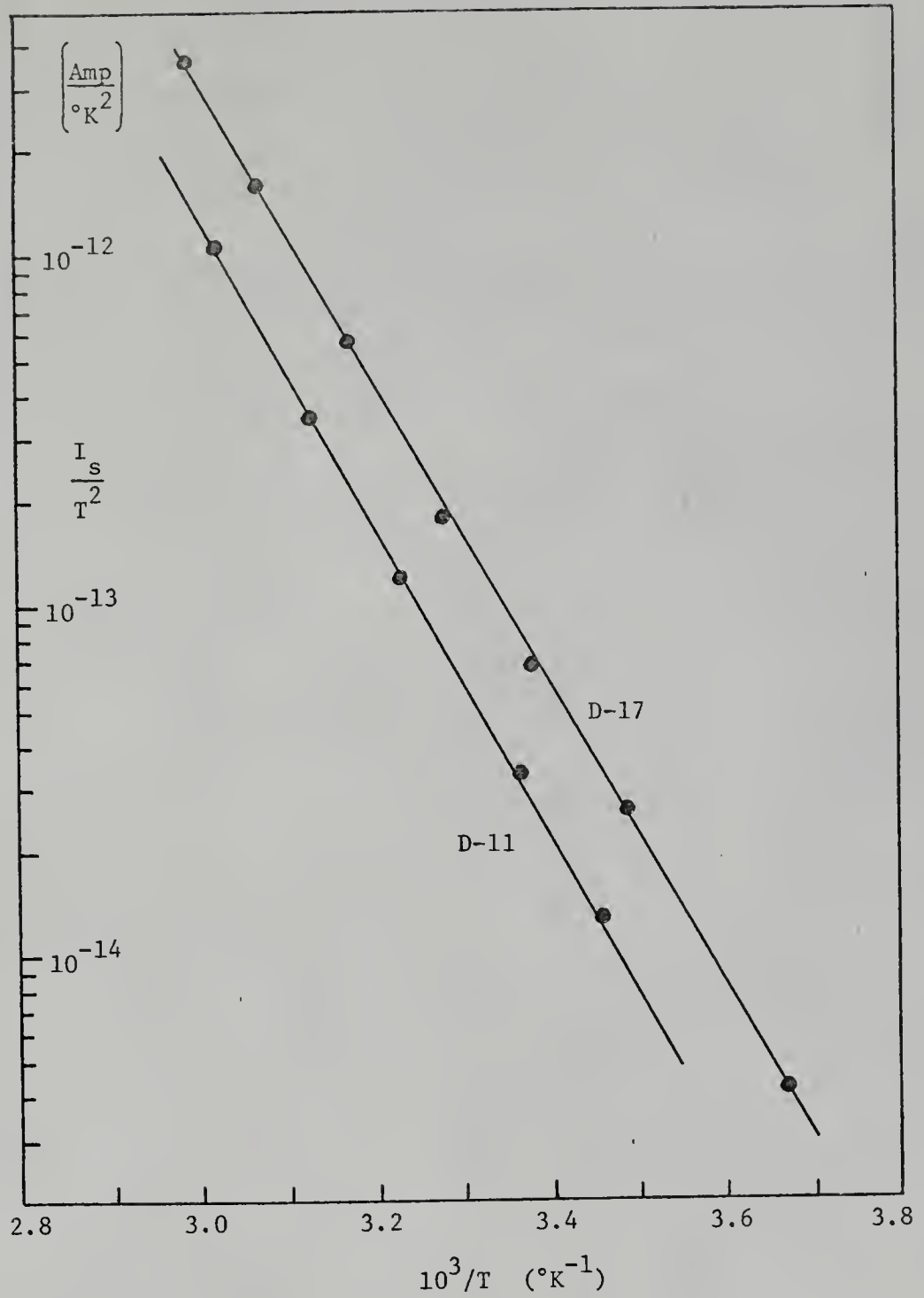


Fig. 11 $\frac{I_s}{T^2}$ versus $10^3/T$ for the Au-GaAs (n-type) Schottky barrier diodes D-11 and D-17.

The Reverse Current-Voltage Measurement of Au-GaAs Schottky Diodes

In Fig. 12, the reverse I-V characteristics for D-17 at 300°K is shown. Experimental data are illustrated by the circles while the solid line represents the theoretical prediction of Eq. (10) with the following parameters:

$$\begin{aligned} N_D &= 2.7 \times 10^{14} \text{ cm}^{-3} & m &= 9 \\ A^* &= 4.4 \text{ amp/cm}^2/\text{°K}^2 & \alpha &= 1.44 \times 10^{-6} \text{ cm} \\ \phi_{bo} &= 0.85 \text{ ev} \end{aligned}$$

For $V > -0.15\text{v}$, the term $\left[\exp\left(\frac{qV}{mkT}\right)-1\right]$ dominates the behavior of reverse-current I . This is in accord with the existence of an interfacial layer. The value of m is related to the thickness of the layer and the equivalent barrier height.²⁷ Instead of solving the complicated tunneling problem, this empirical parameter m serves as a merit factor. For metal-silicide Schottky diodes, the problems of interfacial layer and surface imperfection do not exist and m value is unity.²⁹ For comparison, the prediction with $m = 1$ is also included in Fig. 12.

In the range of higher voltages, the barrier lowering mechanisms dominate the I-V behavior. The value of $\alpha = 1.44 \times 10^{-6} \text{ cm}$ for our device is higher than that of metal-silicide Schottky diodes. This indicates that the dipole layer effect is strong in our device. The dipole layer is thought to be a fundamental consequence of electronic wave function penetration from the metal into the forbidden gap of the semiconductor.²⁹ Perhaps the existence of the deep level impurities has enhanced this effect.

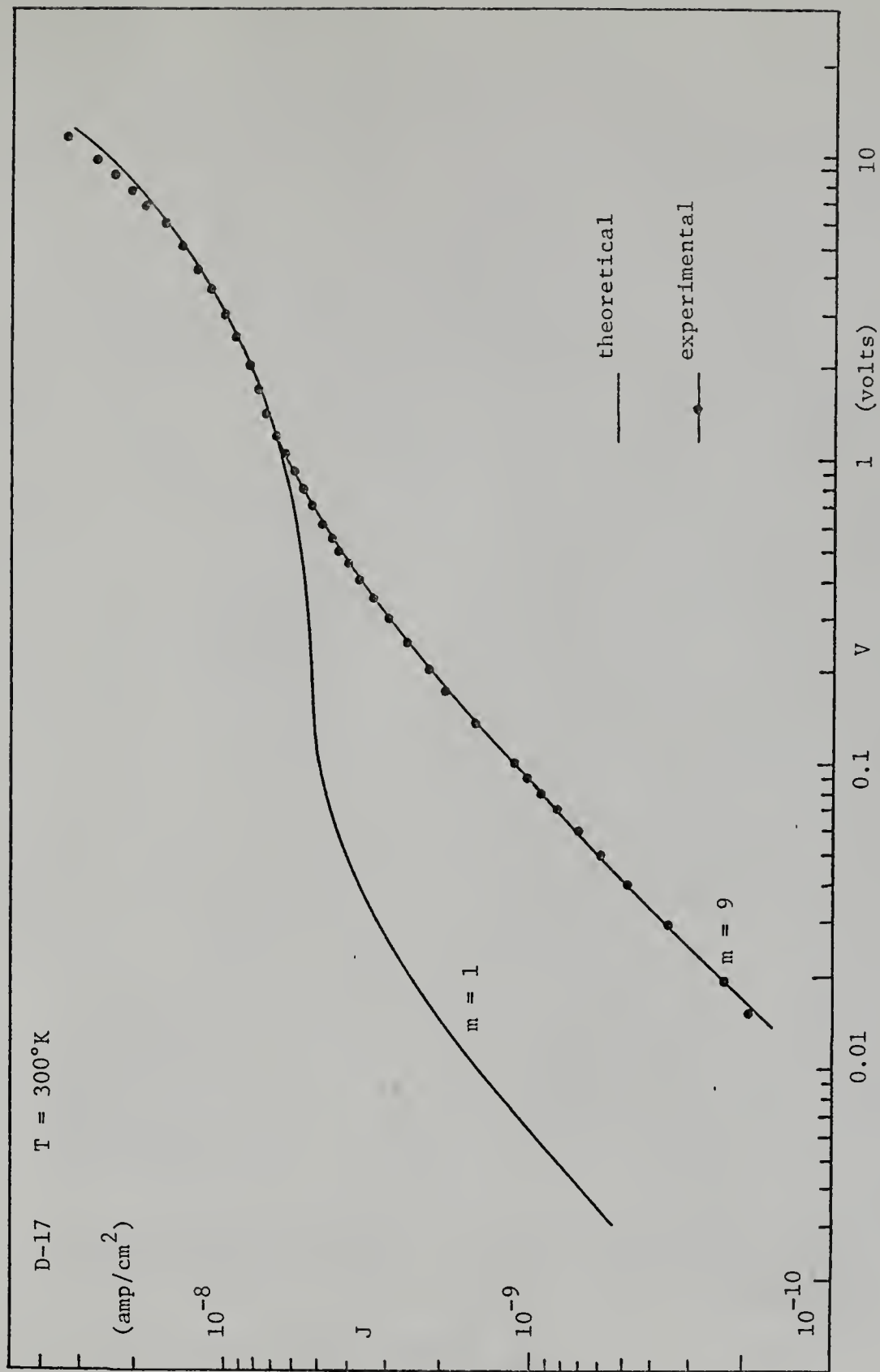


Fig. 12 Reverse voltage-current relationship of Au-GaAs (n-type) Schottky barrier diode D-17.

Transient Capacitance Measurement of Au-GaAs Schottky Diodes

The transient capacitance measurements were performed between 285 and 316°K. A typical capacitance $C = C(t) - C(t=\infty)$ versus time t is illustrated in Fig. 13. In the previous section, the experimental results have indicated the existence of a high resistance interfacial layer in series with the device. Then the measured capacitance C' is⁸

$$C' = \frac{C}{1 + \omega^2 r^2 C^2} \quad (61)$$

where r is the equivalent series resistance. Since $\omega^2 r^2 C^2 < 1$ in our experiments (see a later section), Eq. (24) still can be used to analyze the C-V data without introducing appreciable error.

With the help of the Hewlett-Packard calculator 9100A and the least square curve fitting technique, the time constant (or the reciprocal of the thermal emission rate of electrons), the steady-state capacitance $C(t=\infty)$ and the initial capacitance $C(t=0^+)$ were obtained (Eqs. (25), (26) and (27)).

Field Dependence of Thermal Emission Rate of Electrons

The thermal emission rate of electrons e_n as a function of the average applied electric field is shown for several devices in Fig. 14. At low electric field, the thermal emission rates remain constant for all devices. At higher electric field, the thermal emission rate of Device D-17 shows rapid increase while that of others remains unchanged. This can be explained qualitatively by the Poole-Frenkel effect (field-assisted thermal ionization).³¹

An electron is bound to the deep level impurity atom by some potential which may either be Coulomb's attractive or neutral potential. When an electric field is applied, the effect on the impurity potential

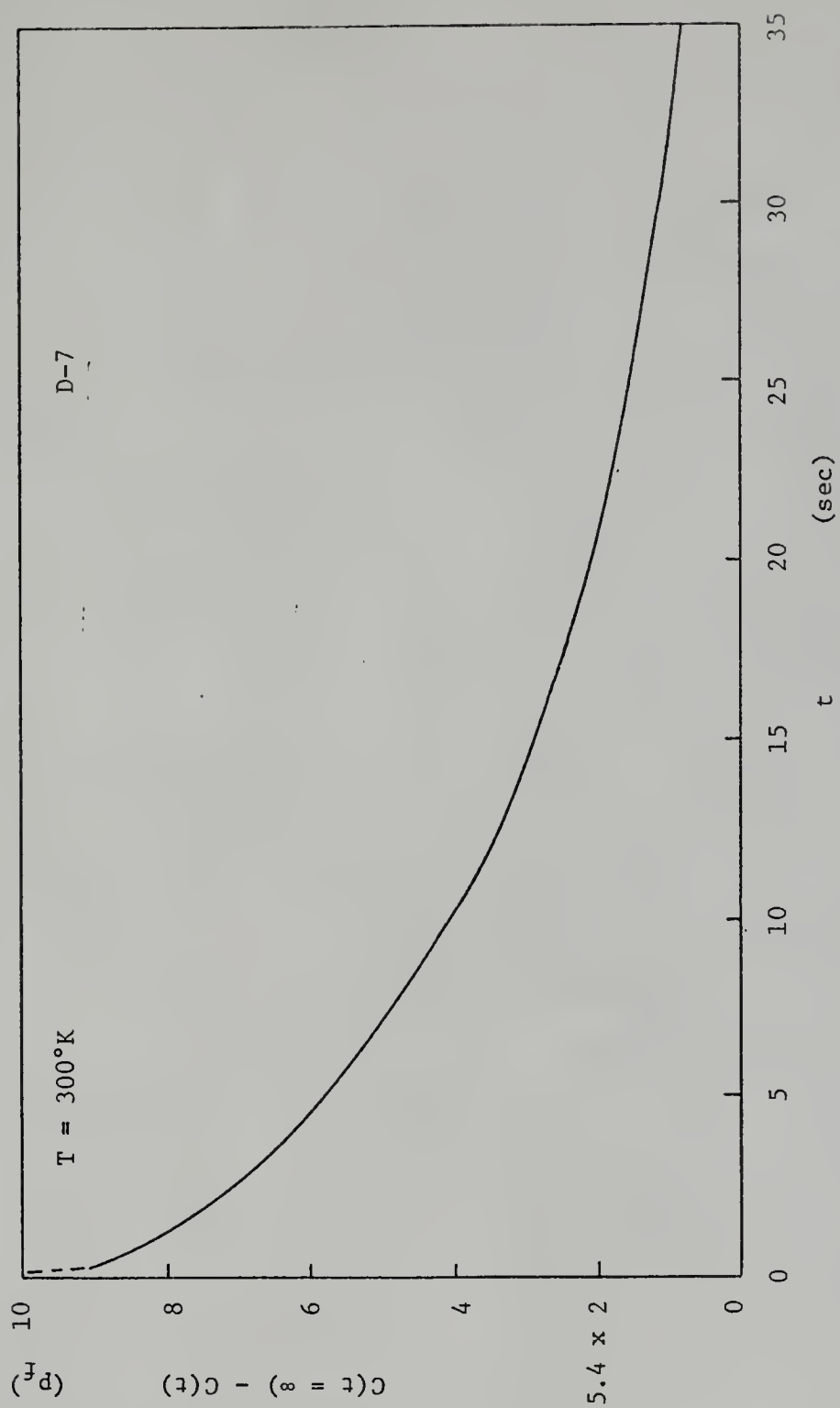


Fig. 13 The actual measured capacitance as a function of time.

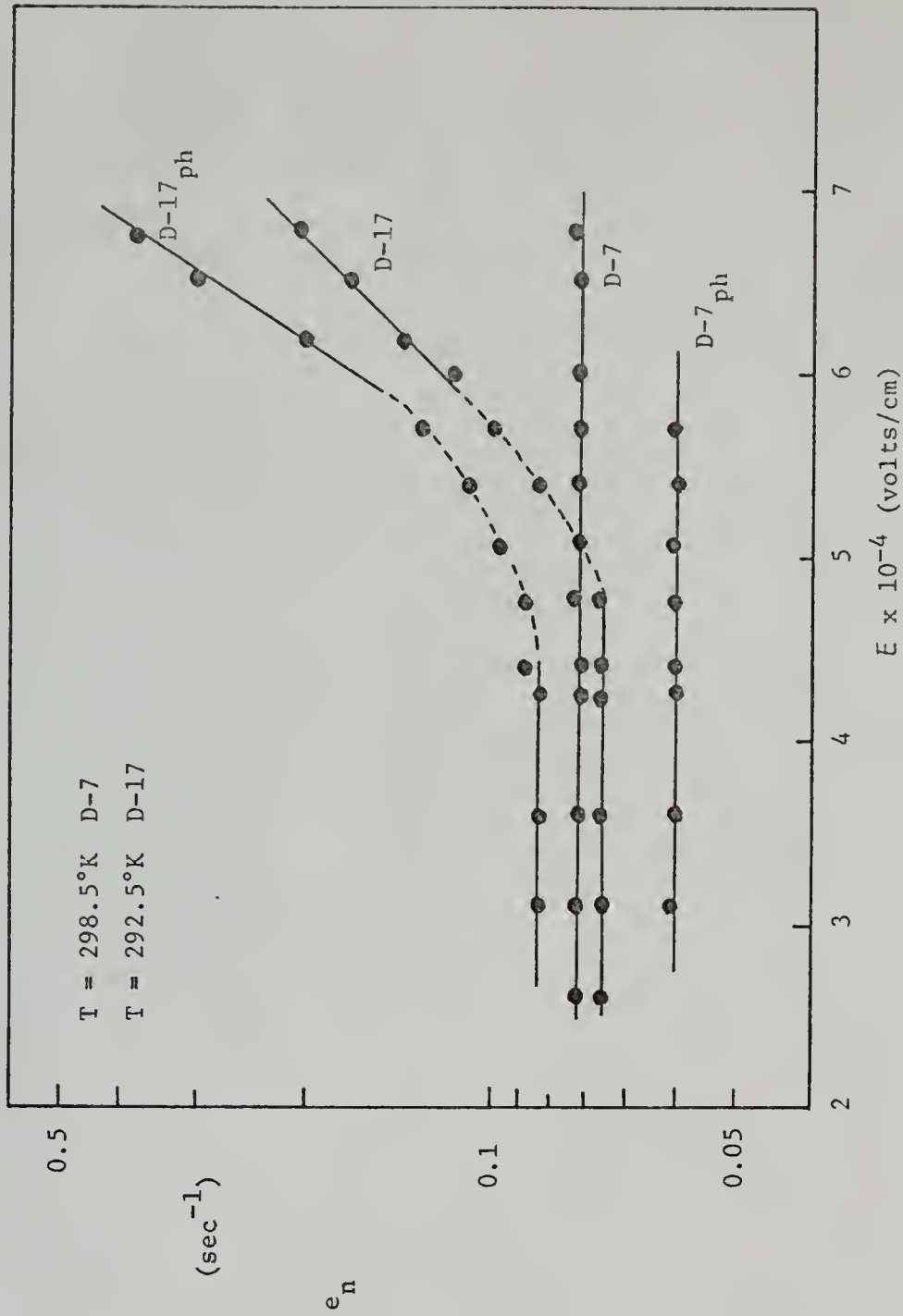


Fig. 14

The thermal emission rate of electrons as a function of average electric field. The subscript ph denotes that the transient photocapacitance method was being employed to obtain the data.

is to lower the barrier that the trapped electron must overcome in order to escape from the deep impurity atom. This then increases the thermal emission rate since it requires less energy to release the electron. It is reasonable to assume that the potential barrier lowering by electric field is more effective on the neutral type potential. This is because of the nature of loose bonding between an electron and the neutral atom. The slighter field dependence of the experimental results of Device D-7 seems to indicate an impurity potential that is more of the Coulomb attractive type. The stronger field dependent thermal emission rate of D-17 favors a neutral type potential. Indeed, the deep impurity in D-7 is the donor-type oxygen.¹⁴ The bonding force between the oxygen atom and an electron is the Coulomb attractive type. While the deep impurity in Device D-17 is an acceptor type chromium,¹⁴ the bonding potential is neutral type. Our experimental results agree with these arguments.

The thermal emission rates of electrons determined by the transient photocapacitance method using interband light ($h\nu > E_g$) are also included in Fig. 14. The slight difference in magnitudes could be due to small temperature variations between two separate measurements. They do indicate similar general trend.

Thermal Activation Energy of Deep Level Impurities

The temperature dependence of the thermal emission rate of electrons is illustrated in Fig. 15. The data were taken at a bias voltage where the emission rate is not field dependent. From Eq. (29) we can determine the thermal activation energy of the deep impurities by calculating the slope of $\ln(e_n)$ versus $1/T$ (see Fig. 15). The results for three devices are

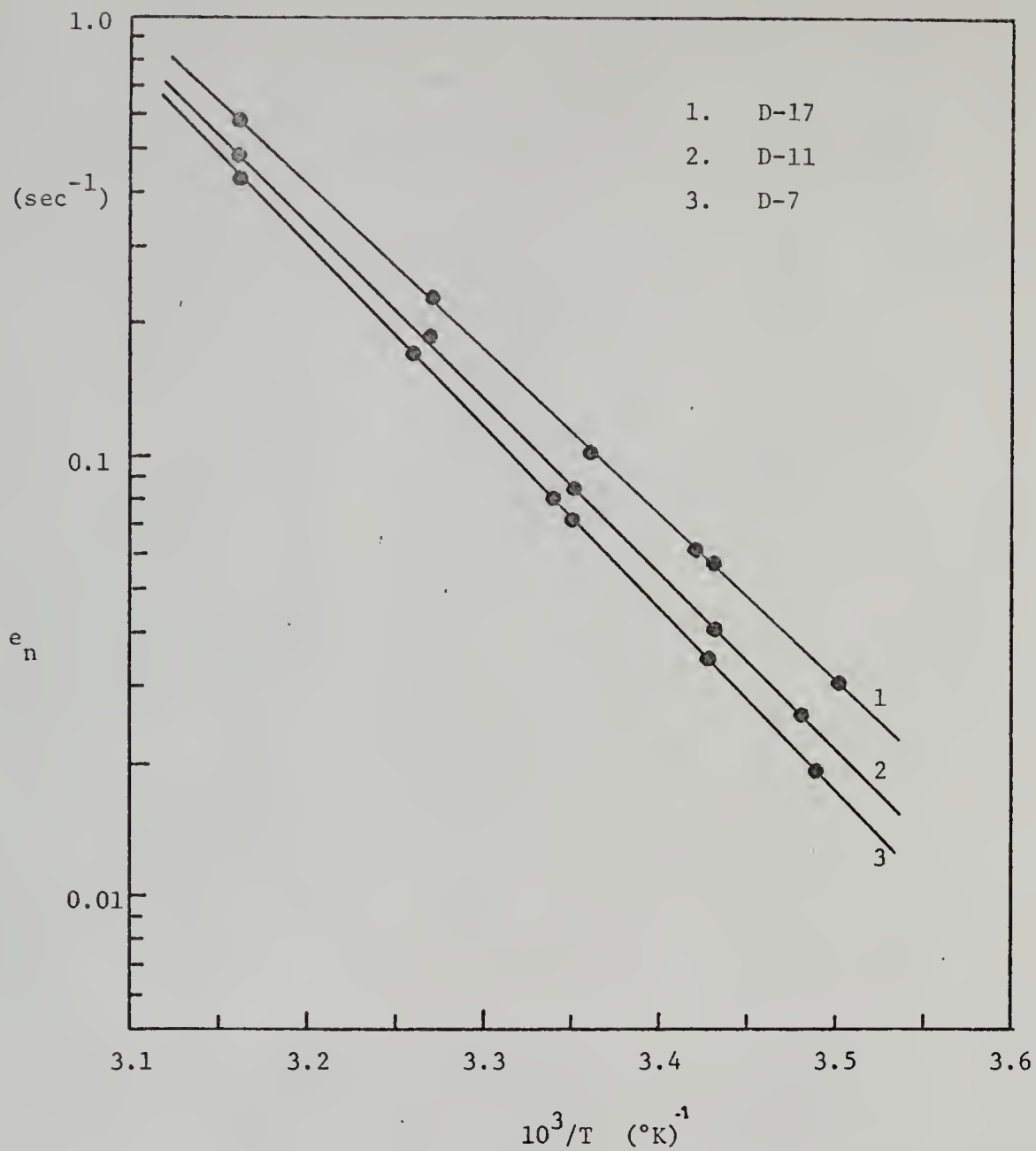


Fig. 15

The thermal emission rate of electron as a function of temperature. ($10^3/T$) between 285 and 316°K. The data were taken at $V = -6$ volts.

D-7 (oxygen) $E_T = 0.82$ ev (from the conduction band edge)

D-11 (oxygen) $E_T = 0.80$ ev

D-17 (chromium) $E_T = 0.74$ ev

Hence, in this measurement we have concluded that the thermal activation energies for oxygen and chromium in GaAs are 0.81 ev and 0.74 ev from the conduction band edge respectively. These values are in good agreement with those obtained by the optical and Hall-effect measurements.¹⁴ They are 0.80 ev and 0.73 ev for oxygen and chromium respectively.

Calculation of Capture Cross Section

Using $v_t = 10^7$ cm/sec, $N_C = 4.7 \times 10^{17}$ cm⁻³ and the values of e_n and E_T determined above in Eq. (29), the electron capture cross section S_n is obtained

$$\text{for chromium impurity} \quad S_n \approx 4.8 \times 10^{-14} \text{ cm}^2$$

and

$$\text{for oxygen impurity} \quad S_n \approx 8.0 \times 10^{-13} \text{ cm}^2$$

These results also reflect the acceptor nature of chromium impurity and the donor nature of oxygen impurity. The capture cross section for oxygen-doped samples determined by the present work is much larger than previously reported values. This is due to the fact that the value of E_T for oxygen in Eq. (29) used by previous authors is considerably smaller than the value we obtained from the present result (for comparisons, see Table II).

Determination of Shallow and Deep Level Impurity Concentrations

The $C(t=0)^{-2}$ versus V and $C(t=\infty)^{-2}$ versus V are shown in Fig. 16 for the devices under study. Although there exists a high resistance

Table 2: Summary of the Results for Au-GaAs (n-type) Schottky Barrier Diodes
Deduced from Transient Dark and Photocapacitance Measurements at 300°K

Author	Deep Level Impurity	E_T (ev)	e_n (sec ⁻¹)	S_n ² (cm ²)	Methods
General Quoted Values ¹⁴	0	0.80	-	-	Hall Effect
	Cr	0.73	-	-	Optical
This work	0	0.81	0.072	8×10^{-13}	C - V
	Cr	0.74	0.065	4.8×10^{-14}	
Zohta ¹³	0.	0.57	-	-	C - V
Furukawa and Ishibashi ¹⁰	0.	0.7	0.06	-	C - V
Williams ⁹	0	0.74	0.15	5×10^{-15}	C - V
Glover ¹²	0.	0.83	-	-	C - V
Senechal and Basinski ¹¹	0.	0.9	-	1.24×10^{-15}	C - V

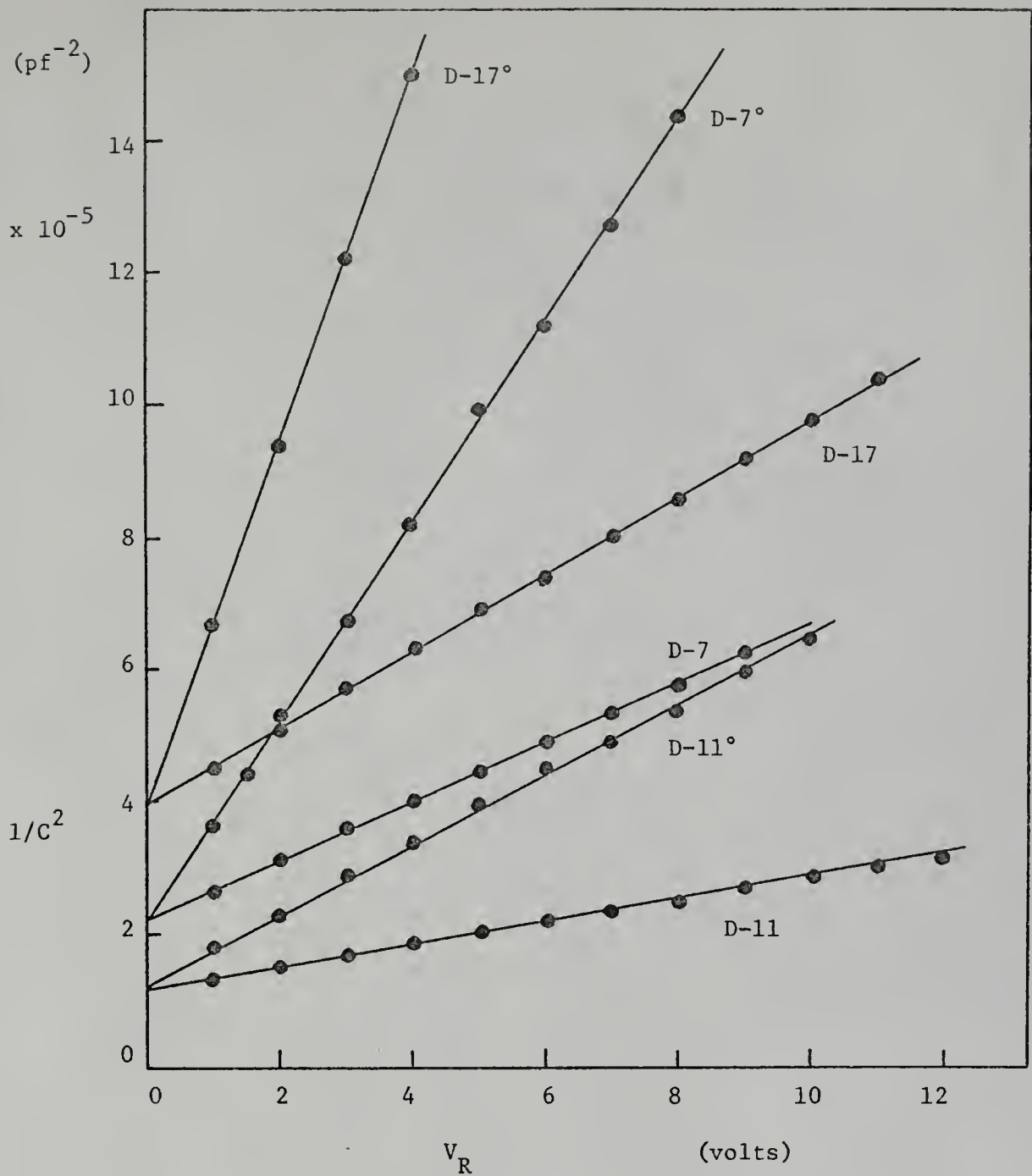


Fig. 16

A plot of C^{-2} as a function of reverse bias voltage for D-17, D-7 and D-11. The superscript $^{\circ}$ represents the values taken at $t = 0^{+}$.

interfacial layer as a series resistor, the slope of C^{-2} versus V still gives the shallow and deep impurity concentrations through Eqs. (25) and (26).⁸ The results are as follows:

$$\begin{array}{ll} \text{for D-7} & N_T = 2.18 \times 10^{15} \text{ cm}^{-3}, \quad N_D = 9.2 \times 10^{14} \text{ cm}^{-3} \\ \text{D-11} & N_T = 5.66 \times 10^{15} \text{ cm}^{-3}, \quad N_D = 2.64 \times 10^{15} \text{ cm}^{-3} \\ \text{D-17} & N_T = 2.03 \times 10^{15} \text{ cm}^{-3}, \quad N_D = 2.55 \times 10^{15} \text{ cm}^{-3} \end{array}$$

Comparing these values with those obtained by our Hall-effect measurement on the bulk n-type GaAs samples, they are in good agreement (see Table 1).

The intercept of the C^{-2} versus V plot on the voltage axis should be the diffusion potential of the diode. However, the existence of a high resistance interfacial layer makes the apparent diffusion potential V'_{bi} higher than the intrinsic value V_{bi} .^{25,41} It has been shown that⁸

$$V'_{bi} = V_{bi} + 2r^2 \omega^2 \left[\frac{d(1/C')^2}{dV} \right]^{-1} \quad (62)$$

From Fig. 16 and Eq. (62), the series resistance r can be estimated ($V_{bi} = 0.9 \text{ eV}$). They are

$$\begin{array}{ll} r \approx 4 \text{ K}\Omega & \text{for D-7} \\ r \approx 3.2 \text{ K}\Omega & \text{for D-11} \\ r \approx 10 \text{ K}\Omega & \text{for D-17} \end{array}$$

These values are much larger than those of the ideal devices. Nevertheless, they have had no appreciable effects on determining the properties of deep impurity centers.

Hall-Effect, Photo-Hall-Effect and Conductivity Measurements

The dark resistivity for chromium-doped semi-insulating GaAs sample S-1 is $1.2 \times 10^8 \Omega\text{-cm}$ and $3 \times 10^8 \Omega\text{-cm}$ for S-2 at 300°K . The Hall

mobility was found to be about $250 \text{ cm}^2/\text{v-sec}$ at 300°K . The low Hall mobility is attributed to the mixed conduction in chromium-doped GaAs occurring at room temperature, as pointed out by Inoue and Ohyama.⁴² The electron mobility can be calculated from the conductivity expression given in Ref. (42), and the result for the present case is found to be $\mu_n = 1000 \text{ cm}^2/\text{v-sec}$ at 300°K . The slight difference in resistivity between S-1 and S-2 implies that the chromium densities are not equal in the two samples. Presumably S-1 has slightly lower chromium impurity density than S-2. This assumption is consistent with the observation of the PME and PC responses in the two samples, in which S-1 shows less trapping effect than S-2.

The photo-Hall-effect measurements over samples indicate that the Hall mobility is a slowly varying function of injection. The photo-Hall experiments in oxygen-doped n-type GaAs samples have been conducted at $T = 4.2^\circ\text{K}$ and 20.8°K respectively. The electron density in these samples measured at 300°K varies from 10^{14} to 10^{15} cm^{-3} . The electron mobility μ_n is $3500 \text{ cm}^2/\text{V-sec}$ at 300°K .

The result of the photo-Hall mobility data is displayed in Fig. 17 for $T = 4.2$ and 20.8°K . Note that the electron mobility is near constant for $\Delta G \leq 10^{-5} \text{ mho}$ but increases with increasing light intensity. The present result shows that μ_n varies with $\Delta G^{0.2}$ for $\Delta G > 10^{-5} \text{ mho}$.

PME and PC Measurement on Chromium-doped n-type GaAs

In Fig. 18, I_{PME}/B versus ΔG for $T = 80$ and 300°K for both S-1 and S-2 is illustrated. It is interesting to note that three well-defined regions are obtained in I_{PME}/B versus ΔG plot. In the high injection region (I), I_{PME}/B is directly proportional to ΔG for S-1 and S-2 at

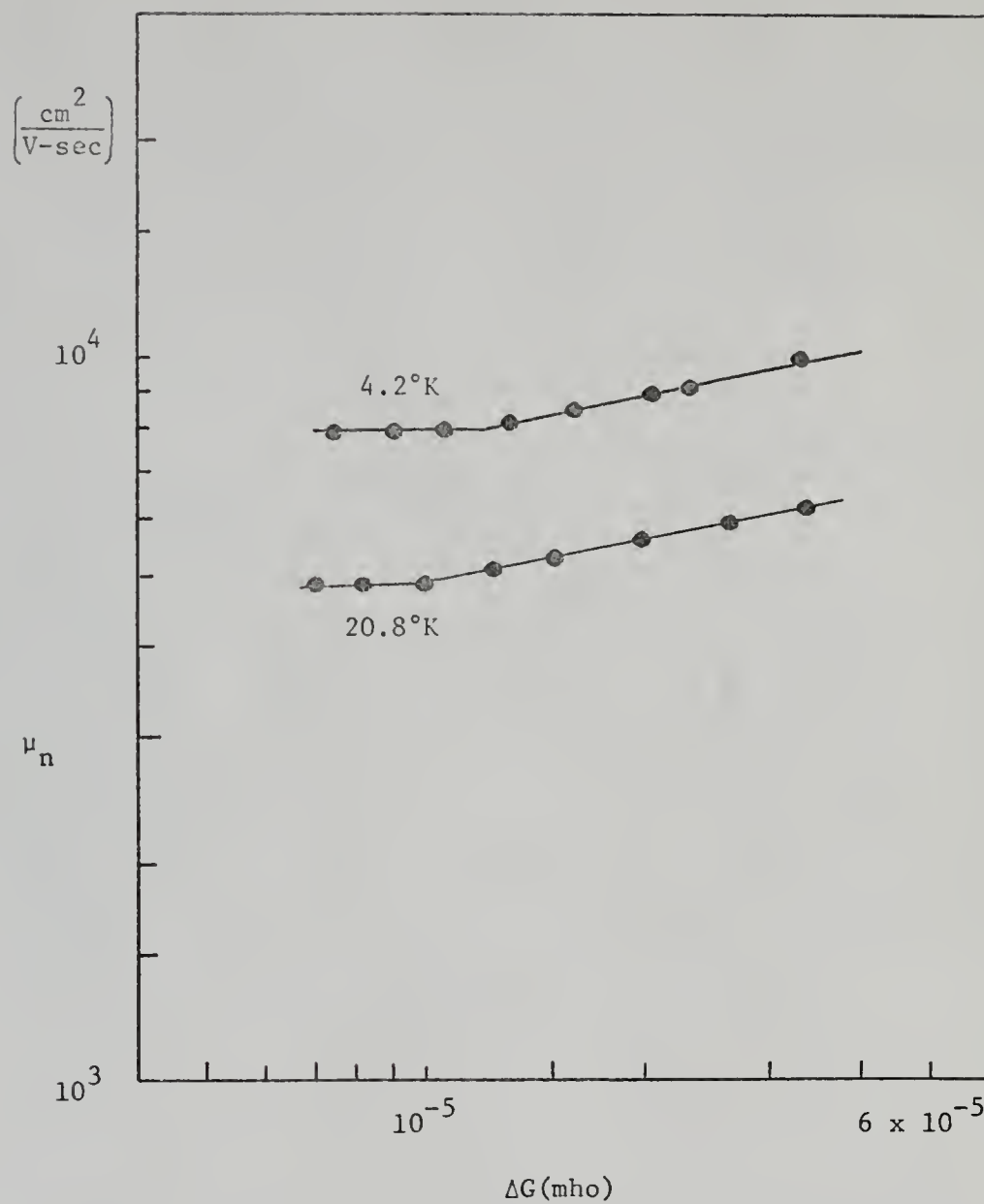


Fig. 17

The photo-Hall mobility versus photoconductance.

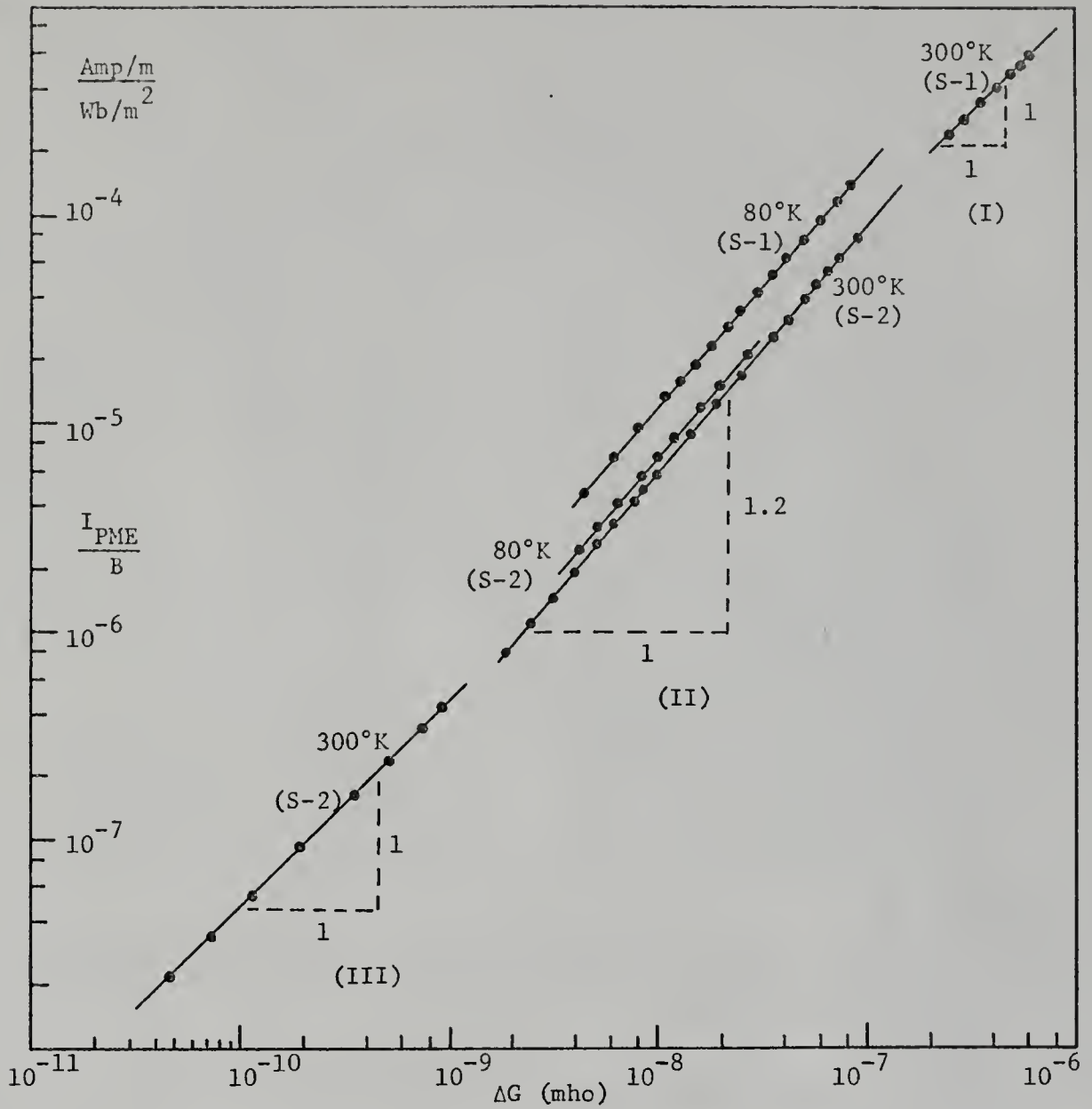


Fig. 18 The PME short-circuit current per unit width of sample per unit magnetic flux density, I_{PME}/B , versus photoconductance ΔG for samples S-1 and S-2 at 80 and 300°K.

300°K. The excess electron and hole densities are much higher than the thermal equilibrium carrier concentration n_0 and the electrically active chromium density. The charge neutrality condition is essentially controlled by the excess electron and hole densities. The carrier lifetime is independent of injection³² and the effect of trapping is completely negligible. As a result, the conditions given by Eqs. (40) and (42) are reduced to

$$\Delta n = \Delta p \quad (\text{i.e. } \Gamma = 1, \ell = 1)$$

and

$$\tau_n = \tau_p = \tau_\infty \quad (\text{i.e. } \beta = 1)$$

where τ_∞ is the carrier lifetime and high injection as defined by Shockley and Read.³² In this case $\tau_n = \tau_p = \tau_\infty = 2.5 \times 10^{-10}$ sec. (Fig. 19).

In the intermediate injection region (II), I_{PME}/B varies with $G^{1.2}$. This is observed for both samples S-1 and S-2 at 80°K and for S-1 at 300°K. The effect of hole trapping at the chromium-acceptor levels ($\Gamma < 1, \ell = 1$), and the dependence of τ_n on $\Delta n^{-1/3}$ leads to the observed relation. Under the conditions of $\ell = 1, \beta = -1/3$ and $\Gamma \neq 1$ Eq. (54) becomes⁴³

$$\tau_a = \left(\frac{42}{25} \right) \left(\frac{7D_p \kappa}{3\Gamma^4} \right)^{1/5} \left(\frac{5\Delta G}{6q\mu_n} \right)^{-2/5} \quad (63)$$

With the help of Eq. (55) τ_p is deduced and the results are shown in Fig. 19. The parameters τ_n, Γ and κ are calculated from Eqs. (42), (54) and (55).

The computed values of Γ and κ are fairly constant over the entire intermediate injection range. The value of Γ is found to be 0.18 at

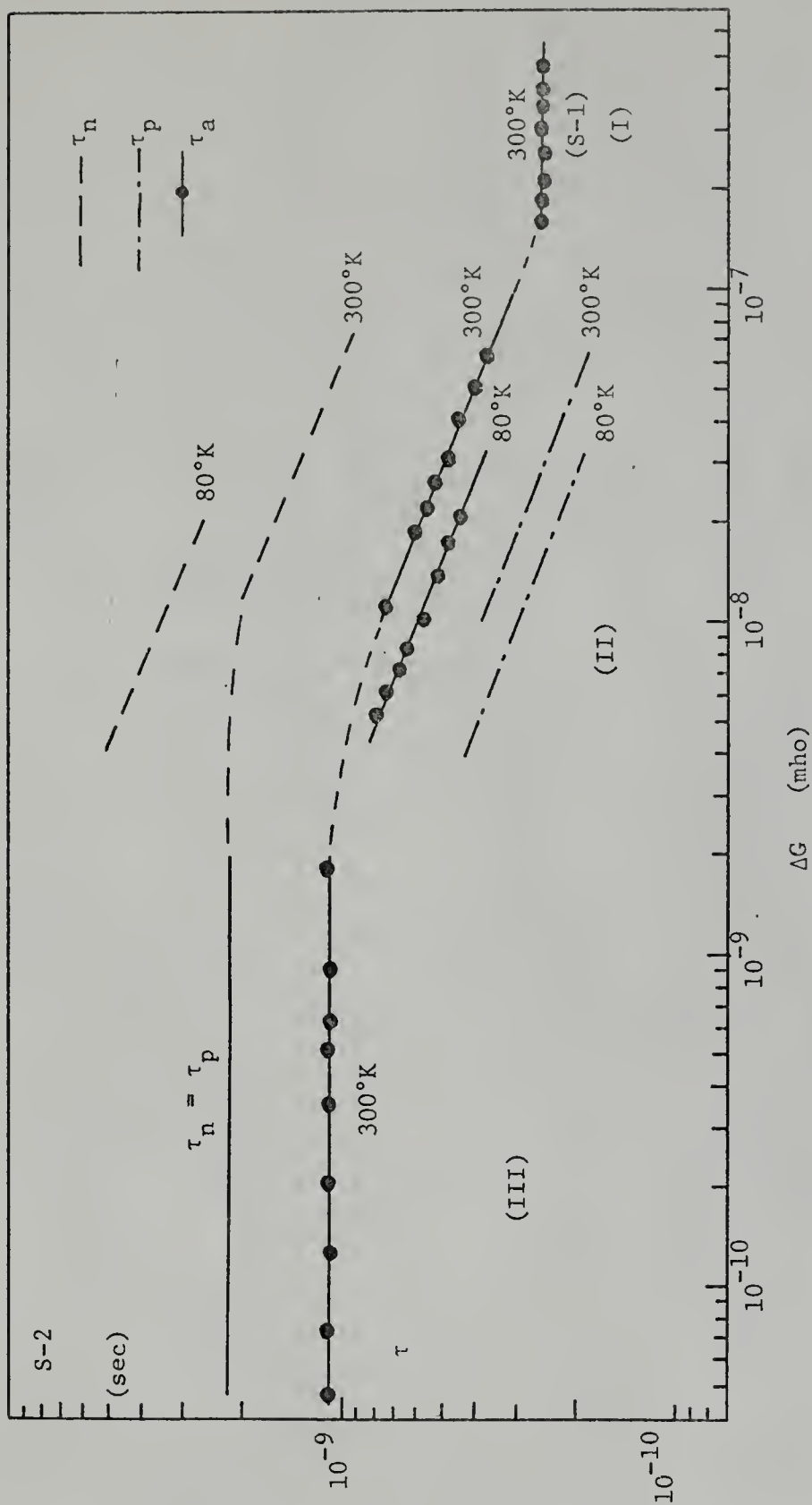


Fig. 19 The PME apparent lifetime τ_a , the electron lifetime τ_n , and the hole lifetime τ_p versus the photoconductance ΔG at 80 and 300°K.

300°K and 0.084 at 80°K for S-2, which shows that the ratio of τ_n/τ_p is about 5.5 at 300°K and about 12 at 80°K. These results are in good agreement with the statement by Holeman and Hilsum¹ in that they predicted a ratio of $\tau_n/\tau_p < 10$ for semi-insulating GaAs.

In the low injection range, another linear region for I_{PME}/B versus ΔG is observed for sample S-2 (Fig. 18). In this region, the effect of trapping is negligible (i.e. $\Gamma = 1$ and $\ell = 1$) and $\beta = 0$. The results are

$$2\tau_a = \tau_n = \tau_p = 2.2 \times 10^{-9} \text{ sec.}$$

This is also included in Fig. 19. The injection (over five orders of magnitude) dependency of carrier lifetimes discussed by Agraz and Li³⁸ has clearly been demonstrated in this experiment.

PME and PC Measurement on Oxygen-Doped N-type GaAs

A plot of I_{PME}/B versus ΔG for $T = 4.2$ and 20.8°K is shown in Fig. 20. From this plot it is found that I_{PME}/B varies with ΔG^2 which is in good agreement with the prediction given by Eq. (56). By using Eq. (58) and data in Figs. 17 and 20, the capture probabilities for band to band radiative recombination are calculated for oxygen-doped n-type GaAs. The results yield

$$B_r = 1.15 \times 10^{-8} \text{ cm}^3/\text{sec at } T = 20.8^\circ\text{K}$$

$$B_r = 1.23 \times 10^{-7} \text{ cm}^3/\text{sec at } 4.2^\circ\text{K}$$

To compare the above experimental values of the capture probabilities with those predicted by Hall's direct radiative recombination formula, we use Eq. (45) to compute B_r for GaAs at 4.2°K and 20.8°K ; the results are

$$B_r = 1.07 \times 10^{-8} \text{ cm}^3/\text{sec at } 20.8^\circ\text{K}$$

$$B_r = 1.18 \times 10^{-7} \text{ cm}^3/\text{sec at } 4.2^\circ\text{K}$$

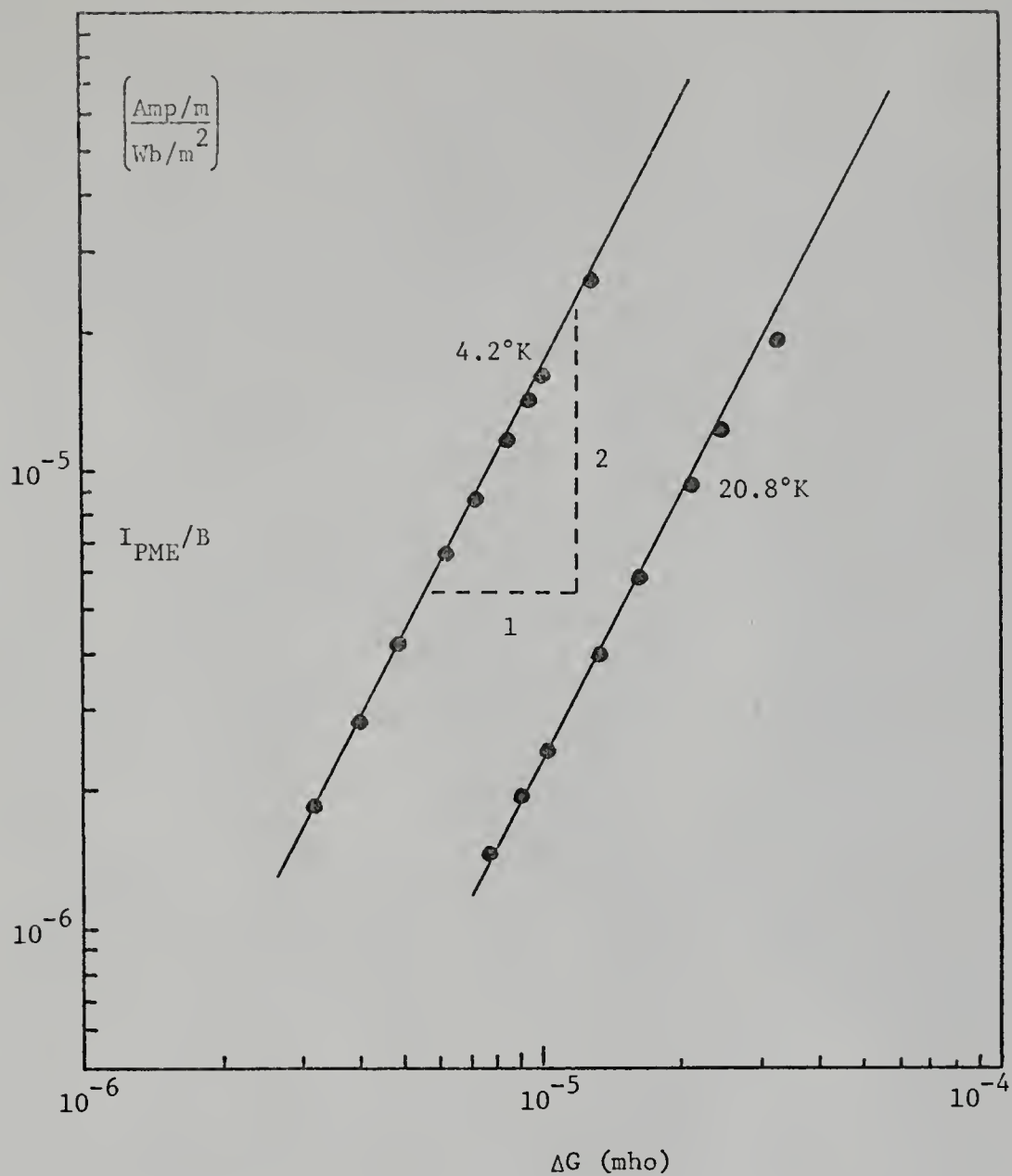


Fig. 20

The PME short-circuit current per unit width of sample per unit magnetic field intensity, I_{PME}/B , versus photo-conductance for oxygen-doped sample S-3 at 20.8 and 4.2°K .

Here $m_e/m_o = 0.068$, $m_h/m_o = 0.5$, and $E_g = 1.51$ eV have been used.

The above result shows that the values of B_r determined from the PME and PC measurements are in excellent agreement with those computed from Hall's direct radiative recombination formula (Eq. (45)). In addition, our results also show that the capture probability B_r depends on $T^{-3/2}$ for the temperature range from 4.2°K to 20.8°K, in accord with the prediction of Eq. (45).

The electron and hole lifetimes can be determined from Fig. 20 and Eq. (53). The result is plotted in Fig. 21. Note that for $\Delta G \leq 10^{-5}$ mho, τ is proportional to ΔG^{-2} in accord with the prediction given by Eq. (57). However, for $\Delta G > 10^{-5}$ mho, τ varies with $\Delta G^{-1.4}$. The change in slope of τ versus ΔG is due to the fact that μ_n also changes with ΔG for high light intensity (i.e., $\mu_n \propto \Delta G^{0.2}$ for $\Delta G > 10^{-5}$ mho).

Estimation of excess carrier density can be obtained from Eq. (3a) of reference (43) for the present case and they are $\Delta n = 2.5 \times 10^{10} \text{ cm}^{-3}$ at 20.8°K and $2.16 \times 10^{12} \text{ cm}^{-3}$ at 4.2°K for $\Delta G = 10^{-5}$ mho. These values are much higher than the equilibrium electron densities at both temperatures. Thus the high injection condition is justified for the present case.

In conclusion, we have shown that the photoinjected excess carrier recombination process in oxygen-doped n-type GaAs at 20.8 and 4.2°K is dominated by the band to band radiative recombination. The deep level oxygen impurities in n-type GaAs are neither acting as recombination centers nor as trapping centers for the excess carriers. The radiative capture probabilities can be determined readily from concurrent measurements of the PME short-circuit current and the photoconductance of the samples.

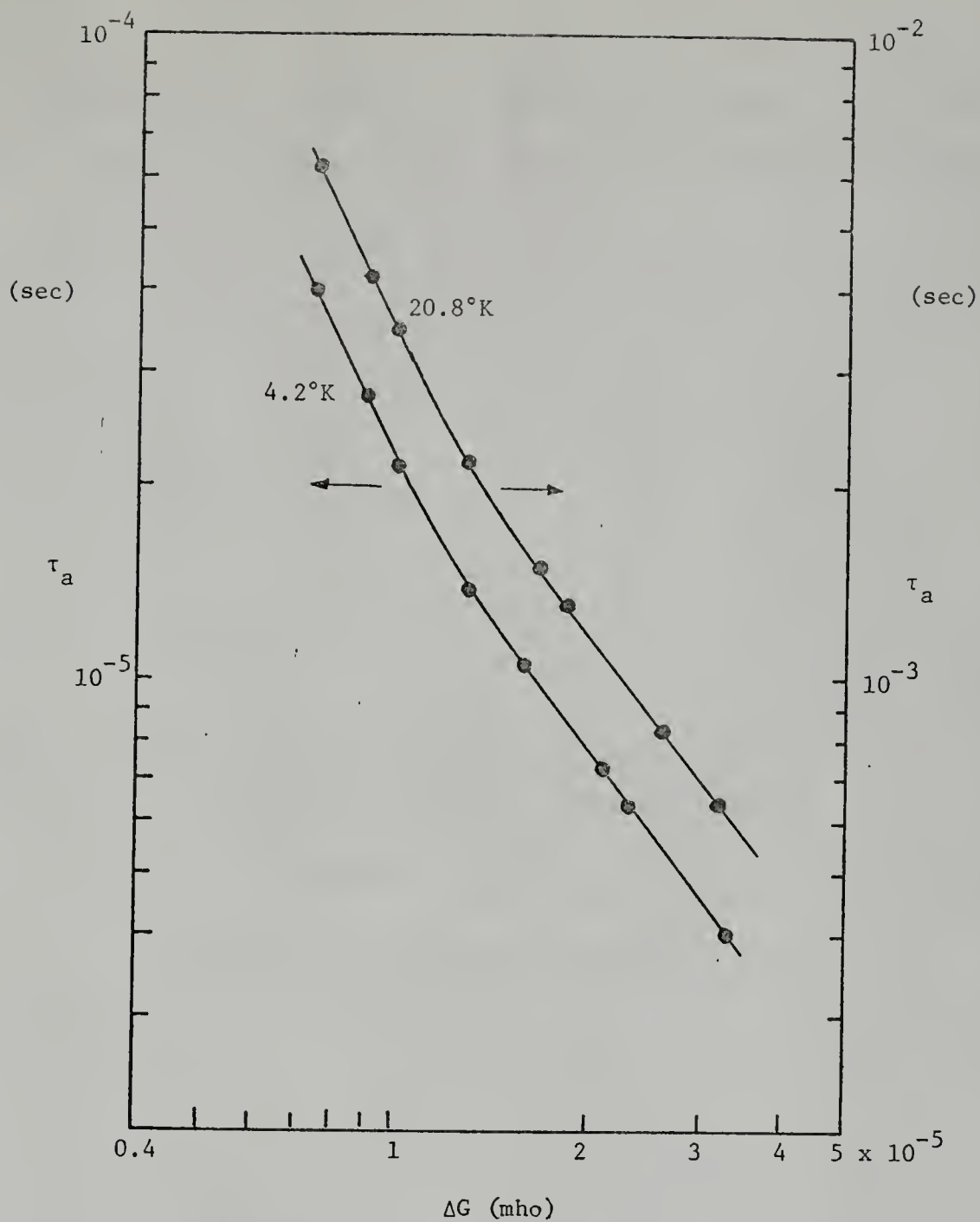


Fig. 21

The PME apparent lifetime τ_a ($\tau_a = \tau_n = \tau_p$) versus photoconductance ΔG for S-3 at 20.8 and 4.2°K .

CHAPTER VII

CONCLUSIONS

Summary

In this work, we have demonstrated a systematic method for characterizing the deep level impurities, oxygen and chromium, in n-type GaAs. The electronic properties of the deep impurity centers are determined by using the transient dark and photocapacitance measurements on the Au-GaAs Schottky diodes. The recombination and trapping parameters are derived from the carrier lifetime measurements. The results are summarized as follows:

- (1) The roles that the deep level impurities, chromium and oxygen, have played in the recombination and trapping processes of the photo-injected carriers in bulk n-type GaAs have been determined by the photomagnetolectric and photoconductive measurements. It is concluded that the chromium impurity centers act as Shockley-Read type recombination centers. On the other hand, the radiative band to band recombination mechanism prevails at low temperatures for n-type GaAs doped with oxygen impurities.
- (2) The experimental results have yielded the dependence of the carrier lifetimes on injected excess carrier densities over a wide injection range in the chromium-doped GaAs. The electron capture probability for the band to band radiative recombination in oxygen-doped GaAs is also obtained experimentally.

(3) The impurity doping concentrations determined by the transient capacitance method are in good agreement with those obtained by Hall-effect measurement (see Table 1).

(4) The thermal emission rates of electrons from negatively charged chromium impurities and neutral oxygen impurities have been measured. They are in the order of 0.07 sec^{-1} (see Table 2). From the temperature dependence of these emission rates, the thermal activation energies for oxygen and chromium in n-type GaAs have been determined. They are 0.81 and 0.74 eV from the conduction band edge for oxygen and chromium levels respectively. These are in good agreement with the values determined by optical and Hall-effect measurements.¹⁴ This kind of accuracy was not achieved by using other transient capacitance models. For comparisons, the results obtained by the previous authors are included in Table 2.

(5) The electric field dependence of the thermal emission rates of electrons was also measured; the results can be explained qualitatively by the Poole-Frankel effect. The present results indicate that oxygen is a donor-type impurity and chromium is an acceptor in nature.

(6) The I-V characteristics have been measured both in forward and reverse bias conditions on the Au-GaAs (n-type) Schottky barrier diodes. From small bias data, it shows the existence of an interfacial layer between gold and GaAs. The intimacy between metal (Au) and semiconductor can be determined experimentally. The field dependence of the effective barrier height also shows up in the form of absence of true saturation in the reverse characteristics. The barrier lowering is caused by the image force and the electrostatic dipole layer in the metal-semiconductor contact. It seems that the dipole layer effect is enhanced by the presence of deep impurities.

(7) The existence of the interfacial layer introduces a high resistance equivalent resistor in series with the Schottky diode. This has prevented the device from having ideal characteristics. However, we can still use the device and transient capacitance method to determine the electronic properties of the deep impurity centers in a semiconductor as we have demonstrated in this work.

Suggestions for Further Study

The results from more extensive study on the transient photo-capacitance, using band to impurity monochromatic photon excitation technique and performed at a temperature below the freeze-out temperature of the deep impurity centers, would be very informative on the optical properties of the oxygen and chromium impurities in GaAs. Combining this information with the excess carrier lifetime measurement over a wide injection range, a complete understanding of the recombination and the trapping mechanisms of excess carriers in GaAs in the presence of oxygen and chromium impurities can be obtained. Furthermore, the experimental techniques presented in this work are applicable to determine the electronic properties of other impurities in GaAs or in other semiconductors.

An experimental study of the PME effect in oxygen-doped GaAs as a function of temperature would also yield the temperature dependence of the electron capture probabilities in the band to band radiative recombination.

BIBLIOGRAPHY

1. B. R. Holeman and C. Hilsum, J. Phys. Chem. Solids, 22, 19 (1961).
2. C. M. Hurd, Proc. Phys. Soc. (London), 79, 42 (1962).
3. R. H. Bube, J. Appl. Phys., 31, 315 (1960).
4. S. Mayburg, Solid State Electron., 2, 195 (1961).
5. T. Kinsel and I. Kudman, Solid State Electron., 8, 797 (1965).
6. R. F. Broom, J. Appl. Phys., 38, 3483 (1967).
7. O. Madelung, Physics of III-V Compounds, (Wiley, New York, 1964).
8. A. M. Goodman, J. Appl. Phys., 34, 329 (1963).
9. R. Williams, J. Appl. Phys., 37, 3411 (1966).
10. Y. Furukawa and Y. Ishibashi, Japan. J. Appl. Phys., 6, 503 (1967).
11. R. R. Senechal and J. Basinski, J. Appl. Phys., 39, 4581 (1968).
12. G. H. Glover, IEEE Trans. Electron. Dev., ED-19, 138 (1972).
13. Y. Zohta, Appl. Phys. Letter, 17, 284 (1970).
14. S. M. Sze and J. C. Irvin, Solid State Electron., 11, 599 (1968).
15. C. T. Sah, L. Forbes, L. L. Rosier and A. F. Tasch, Jr., Solid State Electron., 13, 759 (1970).
16. H. K. Henisch, Rectifying Semiconductor Contacts (Oxford at the Clarendon Press, Oxford, 1957).
17. W. Schottky, Naturwiss. 26, 843 (1938).
18. C. R. Crowell and S. M. Sze, Solid State Electron., 9, 1035 (1966).
19. F. A. Padovani and R. Stratton, Solid State Electron., 9, 695 (1966).
20. A. G. Milnes and D. L. Feucht, Heterojunctions and Metal-Semiconductor Junctions (Academic Press, New York, 1972), p. 163.

21. A. M. Cowley and S. M. Sze, J. Appl. Phys., 36, 3212 (1965).
22. C. A. Mead and W. G. Spitzer, Phys. Rev., 134, A713 (1964).
23. C. R. Crowell, H. B. Shore and E. E. Labate, J. Appl. Phys., 36, 3843 (1965).
24. S. M. Sze, Physics of Semiconductor Devices (Wiley-Interscience, New York, 1969).
25. C. R. Crowell and G. I. Roberts, J. Appl. Phys., 40, 3726 (1969).
26. J. Ohura and Y. Takeishi, Japan. J. Appl. Phys., 9, 458 (1970).
27. J. G. Simmons, J. Appl. Phys., 34, 1793 (1963).
28. G. J. Unterkofer, J. Appl. Phys., 34, 3145 (1963).
29. J. M. Andrews and M. P. Lepselter, Solid State Electron., 13, 1011 (1970).
30. J. A. Copeland, IEEE Trans. Electron Dev., ED-16, 445 (1969).
31. A. F. Tasch, Jr. and C. T. Sah, Phys. Rev. B, 1, 800 (1970).
32. W. Shockley and W. T. Read, Jr., Phys. Rev., 87, 835 (1952).
33. W. van Roosbroeck, Phys. Rev., 101, 1713 (1956).
34. C. T. Sah and W. Shockley, Phys. Rev., 109, 1103 (1958).
35. R. N. Hall, Proc. Inst. Elec. Eng. B. Suppl., 17, 923 (1959).
36. J. Blakemore, Semiconductor Statistics (Pergamon Press, New York, 1962).
37. J. Agraz and S. S. Li, Phys. Rev. B, 2, 1847 (1970).
38. J. Agraz and S. S. Li, Phys. Rev. B, 2, 4966 (1970).
39. R. N. Zitter, Phys. Rev., 112, 852 (1958).
40. S. S. Li, Phys. Rev., 188, 1246 (1969).
41. A. M. Cowley, J. Appl. Phys., 37, 3024 (1966).
42. T. Inoue and M. Ohyama, Solid State Comm., 8, 1309 (1970).
43. S. S. Li and C. I. Huang, J. Appl. Phys., 43, 1757 (1972).

BIOGRAPHICAL SKETCH

Chern I Huang was born May 25, 1940, at Taipei, Taiwan. In June, 1962, he graduated from Cheng-Kung University with the degree of Bachelor of Science in Electrical Engineering. Immediately after graduation he served in the Navy for one year. Following his discharge from the service, he accepted a position at his alma mater as an assistant instructor.

In September, 1964, he started to pursue the graduate study at Iowa State University, Ames, Iowa. He earned the degree of Master of Science in May, 1967. From May, 1966, to August, 1968, he was employed by Collins Radio Company, Cedar Rapids, Iowa, as an engineer. In August, 1968, he moved to Ft. Lauderdale, Florida, to work for Bendix Avionics Division. Since September, 1969, he has worked as a graduate assistant in the Department of Electrical Engineering and has pursued his work toward the degree of Doctor of Philosophy until the present time.

He is a member of the Institute of Electrical and Electronic Engineers. He is married to the former Jennifer Jui-Yu Cheng and is the father of one son.

I certify that I have read this study and that in my opinion it conforms to acceptable standards of scholarly presentation and is fully adequate, in scope and quality, as a dissertation for the degree of Doctor of Philosophy.



Sheng S. Li, Chairman
Assistant Professor of Electrical Engineering

I certify that I have read this study and that in my opinion it conforms to acceptable standards of scholarly presentation and is fully adequate, in scope and quality, as a dissertation for the degree of Doctor of Philosophy.



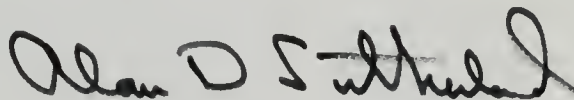
Fredrik A. Lindholm
Professor of Electrical Engineering

I certify that I have read this study and that in my opinion it conforms to acceptable standards of scholarly presentation and is fully adequate, in scope and quality, as a dissertation for the degree of Doctor of Philosophy.



Eugene R. Chenette
Professor of Electrical Engineering

I certify that I have read this study and that in my opinion it conforms to acceptable standards of scholarly presentation and is fully adequate, in scope and quality, as a dissertation for the degree of Doctor of Philosophy.



Alan D. Sutherland
Professor of Electrical Engineering

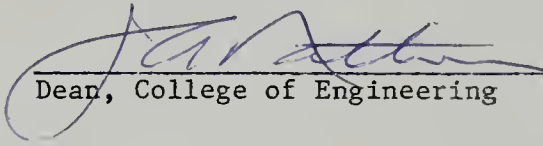
I certify that I have read this study and that in my opinion it conforms to acceptable standards of scholarly presentation and is fully adequate, in scope and quality, as a dissertation for the degree of Doctor of Philosophy.



Thomas A. Scott
Professor of Physics

This dissertation was submitted to the Dean of the College of Engineering and to the Graduate Council, and was accepted as partial fulfillment of the requirements for the degree of Doctor of Philosophy.

March, 1973



Dean, College of Engineering

Dean, Graduate School

37

AM2.9 2108.8.

599616
ABD

(74)